

https://dspace.org/

Optimization of photocatalytic degradation of sulfamethoxazole from wastewater using developed Ndoped TiO2biochar

H Ashebir; Saeideh Babaee; Palesa Diale; A Worku; T.A.M Msagati ...

https://hdl.handle.net/10539/46045
WOS

Downloaded from a DSpace repository. https://dspace.org/

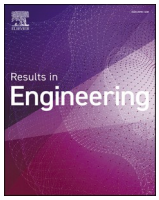
Results in Engineering 26 (2025) 105170



Contents lists available at ScienceDirect

Results in Engineering

journal homepage: www.sciencedirect.com/journal/results-in-engineering



Research paper



Optimization of photocatalytic degradation of sulfamethoxazole from wastewater using developed N-doped TiO_2/biochar

Hailu Ashebir [a,d,*], Saeideh Babaee [b], Palesa Diale [b], Abebe Worku [a], T.A.M. Msagati [c], Jemal Fito Nure [b]

[a] School of Engineering, Department of Environmental Engineering, Addis Ababa Science and Technology University, Addis Ababa, Ethiopia
[b] School of Chemical and Metallurgical Engineering, University of the Witwatersrand, 1 Jorissen St, Johannesburg 2000, South Africa
[c] Institute for Nanotechnology and Water Sustainability (iNanoWS), College of Science, Engineering, and Technology, University of South Africa, Florida Science Campus, Johannesburg 1710, South Africa
[d] Faculty of Biosystems and Water Resource Engineering, Institute of Technology, Hawassa University, Hawassa P.O. Box 05, Ethiopia

ARTICLE INFO

Keywords:
Sulfamethoxazole degradation
Pharmaceutical wastewater treatment
N-doped TiO2/BC nanocomposite
Photocatalysis
Response surface methodology

ABSTRACT

This study introduces a novel N-doped TiO_2/biochar nanocomposite aimed at enhancing the photocatalytic degradation of the antibiotic sulfamethoxazole (SMZ) in pharmaceutical effluent. Utilizing Response Surface Methodology (RSM), key operational parameters were optimized, achieving SMZ's impressive removal efficiency of 98.3 % from synthetic, and 86.6 % from actual wastewater samples. Characterization via X-ray diffraction (XRD) showed a predominant anatase phase, Diffuse Reflectance Spectroscopy (DRS) indicated a bandgap of 2.56 eV, and Fourier Transform Infrared Spectroscopy (FTIR) confirmed nitrogen doping. The optimization involved an agitation period of 95 min, a dosage of 1.5 g/L, a pH of approximately 5, and an SMZ concentration of 110 mg/L. RSM employed Central Composite Design (CCD) comprising four variables and 30 experimental runs to model and analyze degradation process. The quadratic model from RSM exhibited strong statistical significance ($p < 0.0001$) with an R^2 value of 0.9998 and a non-significant lack of fit ($p = 0.3014$), thereby confirming its validity. A close alignment with the pseudo-first-order reaction model was evidenced by a rate constant (k_{app}) of 0.0208 and an R^2 value of 0.991, consistent with the assumptions of the Langmuir-Hinshelwood model. Notably, this study successfully developed a highly durable nanocomposite (sustaining >6 cycles with <5 % efficiency loss), and displayed 1.58 times greater activity under visible light compared to pristine TiO_2 and effectively degraded 95 % of pharmaceutical residues within just 30 min, significantly surpassing the 64.2 % degradation rate of bare BC. This demonstrates the nanocomposite's potential as a scalable and energy-efficient solution for wastewater treatment.

1. Introduction

Pharmaceutical residues in wastewater have become a significant environmental concern, attracting considerable attention from researchers, policymakers, and environmental advocates due to their persistence, potential for bioaccumulation, and contribution to antibiotic resistance [1–3]. Sulfamethoxazole (SMZ), a commonly used sulfonamide antibiotic, is a significant environmental concern due to its persistence as a contaminant [4,5]. Its chemical stability and resistance to standard wastewater treatment methods enable it to remain in aquatic environments for extended periods, making it a widespread pollutant in water systems around the world [6]. The primary sources of SMZ pollution are varied and include hospital effluents that release unmetabolized antibiotics through patient waste, pharmaceutical manufacturing facilities that discharge untreated or partially treated waste, and agricultural runoff, where SMZ enters water bodies from manure applied to fields by livestock that have been treated with the antibiotic [3,7,8]. The pathways through which SMZ enters rivers, lakes, and groundwater contribute to its widespread presence, posing significant ecological and public health risks [1,9]. Once SMZ is introduced into aquatic ecosystems, it disrupts microbial communities that are essential for maintaining ecological balance. Additionally, it directly threatens aquatic organisms, such as fish and invertebrates, by interfering with their physiological processes and reproductive systems.

* Corresponding author.
E-mail address: ashebirhailu@gmail.com (H. Ashebir).

https://doi.org/10.1016/j.rineng.2025.105170
Received 1 February 2025; Received in revised form 28 March 2025; Accepted 30 April 2025
Available online 1 May 2025
2590-1230/© 2025 The Authors. Published by Elsevier B.V. This is an open access article under the CC BY-NC-ND license (http://creativecommons.org/licenses/by-nc-nd/4.0/).

Perhaps most concerning is the persistent presence of SMZ in water bodies, accelerating the development and spread of antibiotic-resistant bacteria. This poses a global health crisis that undermines the effectiveness of life-saving antibiotics [10]. Conventional wastewater treatment methods, including biological degradation [11], chemical oxidation [12], and physical filtration, have proven inadequate in completely removing SMZ and other pharmaceutical residues [13–15]. These techniques often struggle to break down the complex molecular structures of these contaminants, which allow them to pass through treatment plants and enter natural water systems [16].

Several advanced treatment technologies, which go beyond conventional methods, have been investigated to effectively remove pharmaceutical residues and other micropollutants from wastewater [17]. Among these technologies, adsorption [18], ozonation [19], and membrane filtration [20] have been widely applied. However, each method has significant limitations that impact its efficiency, sustainability, and practicality for large-scale applications [21]. Adsorption, particularly using activated carbon or biochar, is one of the most common approaches due to its simplicity and effectiveness in capturing pollutants. However, it is important to note that adsorption is a non-destructive process; it merely transfers contaminants from the water phase to a solid medium without degrading them [22]. There is a need for frequent regeneration or disposal of adsorbents, which leads to concerns about secondary pollution and increased operational costs [23]. Ozonation is a widely used oxidative treatment method that effectively degrades pharmaceutical compounds by breaking down their molecular structures through reactions with ozone. While ozonation can significantly reduce the concentration of pollutants, it does not always achieve complete mineralization, resulting in potentially toxic byproducts [24]. For instance, harmful byproducts such as sulfanilic acid ($C_6H_7NO_3S$) and 3-amino-5-methylisoxazole ($C_4H_6N_2O$) have been identified in the case of SMZ; some of these byproducts exhibit antimicrobial activity and may contribute to the selection of antibiotic-resistant strains [25–27]. The process is energy-intensive, incurs high operational costs, and requires careful control to prevent the formation of nitrosamines and bromate, both of which are known carcinogens. Membrane filtration techniques, such as nanofiltration and reverse osmosis, provide a physical method for removing pharmaceutical contaminants [13]. However, membranes are highly prone to fouling, which necessitates frequent maintenance and replacement. Additionally, while membrane processes do not degrade contaminants, they concentrate them into reject streams, which can pose disposal challenges and potential environmental risks [28,29]. The presence of natural organic matter, scaling agents, and bio-fouling compromises long-term membrane performance [30]. There is an urgent need for advanced treatment technologies to remove and completely degrade pharmaceutical contaminants like SMZ to protect aquatic ecosystems and public health [31]. Advanced oxidation processes (AOPs), particularly heterogeneous photocatalysis, show promise by generating reactive radicals that break down organic pollutants into harmless products like CO_2 and H_2O [32,33]. Unlike conventional methods, photocatalytic processes are sustainable, chemical-free, and energy-efficient, offering a viable alternative for addressing pharmaceutical pollution in wastewater [34,35].

TiO_2-based photocatalysis has gained considerable attention as a promising method for degrading pharmaceutical residues due to its strong oxidative properties, chemical stability, and low toxicity [36,37]. However, its practical application in wastewater treatment faces several challenges that hinder scalability and efficiency. One major limitation is the wide bandgap of TiO_2 (approximately 3.2 eV for the anatase form), which restricts its light absorption to the ultraviolet (UV) region, capturing only about 5 % of the solar spectrum [38,39]. This significantly limits its effectiveness under natural sunlight, making it energy-intensive and costly for large-scale applications. Furthermore, TiO_2 experiences rapid electron-hole recombination. This occurs when the charge carriers generated during photon absorption recombine before they can participate in redox reactions, which greatly reduces the photocatalytic efficiency [40]. To tackle these challenges, researchers have investigated strategies such as doping TiO_2 with nonmetals like nitrogen, sulfur, or carbon. This approach helps to narrow its bandgap and enhance visible light absorption. Another promising strategy is to combine TiO_2 with conductive materials, such as biochar (BC), which not only improves charge separation but also increases adsorption capacity, thus enhancing overall photocatalytic performance [41]. However, despite these advancements, the practical application of TiO_2-based photocatalysis continues to be limited by the lack of scalable and adaptable solutions for real-world wastewater treatment. This study aims to address these issues by synthesizing and optimizing an N-doped TiO_2/BC nanocomposite using the sol-gel method. This approach is designed to improve visible light activity and reduce electron-hole recombination, ultimately enhancing the overall efficiency of SMZ degradation. Although modified TiO_2 composites show promising potential, there are still significant research gaps, particularly regarding the complexities of real wastewater systems [42]. Most studies have focused on batch-scale experiments in controlled laboratory conditions, optimizing variables like pollutant concentration, pH, and light intensity in isolation. However, real wastewater is more complex, containing fluctuating levels of SMZ, competing ions (nitrates, chlorides, sulfates), and various organic and inorganic contaminants that can affect photocatalytic efficiency [43]. The interactions among these factors and their influence on TiO_2-based photocatalysis have not been extensively researched, limiting the application of laboratory findings to real-world scenarios. While biochar-TiO_2 composites show improved performance due to biochar's ability to adsorb pollutants and enhance electron transfer, their long-term stability and reusability in dynamic environments remain underexplored [44,45]. This study evaluates the photocatalytic performance of nitrogen-doped TiO_2/BC composites using Response Surface Methodology (RSM) and Factorial Experimental Design. It focuses on key parameters SMZ concentration, pH, contact time, and light intensity [46–48], to identify optimal conditions for SMZ degradation and bridge the gap between lab results and practical wastewater treatment applications.

To address gaps in wastewater treatment, future research should focus on developing scalable and adaptable photocatalytic technologies that consider the complexities of real wastewater [49]. This includes creating durable, N-doped TiO_2/BC nanocomposites that perform well under visible light and withstand environmental changes. It's essential to evaluate these materials within existing treatment systems while ensuring cost-effectiveness, long-term stability, and reusability. This study examines the practical application of the nanocomposite under real sunlight, addressing a key gap in previous research that relied on artificial UV sources. By designing an optimized and affordable photocatalytic system, this research advances water treatment technologies and aligns with global efforts to enhance sustainability and reduce pharmaceutical pollution in aquatic environments. The findings are expected to significantly contribute to developing next-generation systems that can effectively tackle pharmaceutical residues in wastewater, supporting environmental and public health goals.

2. Methods and materials

2.1. Chemicals

In this research, all chemicals and reagents used were of laboratory grade and sourced from various manufacturers and suppliers. To synthesize the N-doped TiO_2/BC nanocomposite, titanium (IV) isopropoxide (TTIP) with a purity of 97 % was utilized as the source of TiO_2. This reagent was sourced from Sisco Research Laboratory Pvt. Ltd. in New Mumbai, India. Other essential reagents that supported the synthesis process included absolute ethanol (99.9 %), silver nitrate ($AgNO_3$), and ethylene diamine tetra-acetic acid (EDTA), which were all procured from import companies in Addis Ababa, Ethiopia. Additionally, extra pure isopropanol (99.99 %) was supplied by Sisco Research

Laboratory and was obtained from Addis Ababa Science and Technology University (AASTU). This reagent was used for experiments conducted at the AASTU laboratory. Titan Biotech Ltd., located at the AASTU facility, supplied the extra pure urea, which had a purity of 99.8 %. We obtained 100 % pure SMZ for the pharmaceutical analysis from the Ethiopian Pharmaceutical Manufacturing S.C., which is part of the governmental sector. All chemicals and reagents used in this study were of laboratory quality and did not require any additional purification. The BC used in this study was produced from the biomass of the invasive weed Prosopis Juliflora (PJ), collected from the Afar Regional State in rural Ethiopia. This biomass was chosen due to its high availability and potential for resource recovery. Our previous work included a comprehensive synthesis process for this biochar [50].

2.2. Photocatalytic reactor setup

The photocatalytic degradation experiments were conducted using a custom-designed batch reactor. This reactor was equipped with a 19 W/cm^2 UV lamp emitting light at a controlled wavelength of 278 nm, which is optimal for activating the N-doped $TiO_2/BC_{20\ \%}$ nanocomposite. The lamp was positioned 5 cm above the solution, which was stirred by a magnetic stirrer inside a covered box. To improve light utilization, the reactor featured a reflective interior surface [51]. The temperature during the experiments was maintained at approximately 25 °C, consistent with Ethiopia's winter season, and natural air circulation was allowed. The reaction mixture was continuously stirred at 150 rpm to ensure uniform dispersion of the photocatalyst and prevent settling. A digital pH meter (HI2020–01 edge® Multiparameter pH Meter) was used to monitor and adjust the pH of the reaction mixture. To adjust the pH, dilute HCl or NaOH solutions were used. The pH meter was calibrated daily with standard buffer solutions to ensure accuracy. The equipment used to measure the absorbance during the degradation of SMZ was a UV–Vis spectrophotometer, which monitored the reaction mixture at a specific wavelength of 278 nm. Sampling occurred every 15 min, and spectrophotometric analysis was performed to quantify the concentration of SMZ throughout the degradation process. The primary instrument for this analysis was Liquid Chromatography-Mass Spectrometry (LC-MS), which identified and quantified SMZ and its degradation byproducts. The LC-MS provided valuable insights into the chemical transformations occurring during photocatalytic degradation, including the detection of intermediate compounds. Samples were filtered and prepared according to LC-MS protocols to ensure accurate measurements [52]. Additionally, the instrument's operational parameters, such as mobile phase composition and flow rate, were optimized for the analysis of SMZ.

2.3. Synthesis of N-Doped TiO_2/BC nanocomposite

The N-doped TiO_2/BC nanocomposite was synthesized using a modified sol-gel method aimed at integrating bacterial cellulose (BC) with nitrogen-doped TiO_2. The procedure was carefully optimized to produce a uniform composite material with enhanced photocatalytic properties. To initiate the synthesis, 50 mL of absolute isopropanol and 50 mL of absolute ethanol were combined in a round-bottomed beaker. This mixture was stirred constantly (at 450 rpm) at room temperature until it became homogeneous. Once the solution was uniform, 10 mL of TTIP was added dropwise to the mixture, maintaining similar stirring conditions. This addition was performed slowly to prevent premature hydrolysis, and the mixture was stirred for an additional 30 min to ensure uniform dispersion of the TTIP. The next step involved preparing the BC, which was then added to the sol-gel mixture in predetermined proportions. The mass ratio of BC to TTIP was varied to create samples with different BC contents for material optimization (10 %, 20 %, 30 %, 40 %, and 50 %). After adding the BC, the mixture was stirred for another 30 min to ensure thorough integration of the BC into the precursor solution. Finally, the solution was heated to 80 °C on a hotplate while being continuously stirred. This step facilitated the gelation process, which typically took about 2 hrs [50]. During this time, the solvent gradually evaporated, transforming the mixture into a thick gel with a light-yellow appearance. The gel was then transferred to an oven and dried at 105 °C for 24 hrs to remove residual moisture and solvents. This drying process resulted in a solid material that was subsequently crushed into a fine powder using a mortar and pestle. The dried material was calcined at 600 °C for 2 hrs in a muffle furnace under a flow of nitrogen gas. The heating rate was maintained at 10 °C per minute to ensure the gradual decomposition of organic components and uniform crystallization of TiO_2. The nitrogen doping mechanism was investigated using urea as the nitrogen source. Its inclusion ensured effective doping during the calcination step, promoting nitrogen incorporation into the TiO_2 lattice and enhancing the visible light absorption capabilities of the photocatalyst. Additionally, this process improved the adhesion between the TiO_2 matrix and the BC, which served as both a dopant and a complementary material [53]. To introduce nitrogen into the TiO_2 lattice, urea was added during the initial sol-gel preparation stage, before incorporating the BC. The synthesized nanocomposite was labeled as N-doped TiO_2/BCx, where x represents the percentage of BC relative to TTIP (e.g., N-doped $TiO_2/BC_{10\ \%}$, N-doped $TiO_2/BC_{20\ \%}$, etc.). A pure TiO_2 sample was also synthesized using the same sol-gel method but without adding BC and urea, serving as a control for comparison instead of using commercial TiO_2.

2.4. Experimental design

A systematic approach to experimental design was utilized to optimize the photocatalytic degradation of SMZ using an N-doped $TiO_2/BC_{20\ \%}$ nanocomposite. The study examined four key variables: initial SMZ concentration, pH, contact time, and nanocomposite dosage, each assessed at multiple levels (low, medium, and high). To enhance the analysis, a Central Composite Design (CCD), a subset of RSM, was implemented. A quadratic model was selected for the RSM framework because preliminary experiments and prior research revealed non-linear interactions among critical process parameters, including catalyst dosage, pH, and reaction time. This quadratic model effectively captures second-order interactions, thereby improving predictive accuracy. While the Box-Behnken Design (BBD) is effective in minimizing experimental runs, it does not encompass extreme factor levels, which are vital for fully understanding the photocatalytic degradation process. Furthermore, model adequacy tests affirmed that the quadratic model yielded a high R^2 value and an insignificant lack-of-fit, validating its appropriateness. Consequently, the quadratic model was chosen to ensure a more precise and comprehensive optimization of SMZ degradation. This approach enabled an in-depth exploration of factor interactions and their non-linear effects, providing a solid foundation for identifying optimal conditions [54]. The primary response variable was the percentage degradation of SMZ, determined through periodic monitoring of its concentration. Analytical measurements were conducted using a UV–Vis spectrophotometer at 278 nm, supplemented by LC-MS for a detailed analysis of degradation products and mineralization. This methodology ensured a thorough optimization and statistical validation of the photocatalytic process.

2.5. Photocatalytic experiment

The photocatalytic degradation experiments were conducted in a batch reactor system designed to ensure uniform mixing and controlled light exposure. The reactor was equipped with a magnetic stirrer to maintain a consistent reaction mixture and prevent the settling of the N-doped $TiO_2/BC_{20\ \%}$ nanocomposite. Illumination was provided by two light sources: a UV light source to activate the photocatalyst and natural sunlight to evaluate performance under real-world conditions. To block interference from ambient light during UV experiments, the reactor chamber was covered. Key reaction parameters were systematically

modified to study their effects on the degradation of targeted pollutants. The pH of the reaction mixture was adjusted using dilute NaOH or HCl solutions, with a range from 3 to 9, to investigate the influence of acidic, neutral, and alkaline conditions. SMZ solutions with varying concentrations between 5 and 150 mg/L were prepared by dissolving the compound in deionized water to mimic pharmaceutical contaminants at different levels. The dosage of the N-doped $TiO_2/BC_{20\ \%}$ nanocomposite was optimized within a range of 0.1 to 2 g/L to achieve a balance between catalytic efficiency and material usage [55]. Reaction times were varied from 15 to 120 min to observe the kinetics of the degradation process [9]. Control experiments were conducted to confirm the photocatalytic activity of the nanocomposite. These included tests performed in the absence of a catalyst and under dark conditions, ensuring that any degradation was not due solely to photolysis or adsorption [56]. The control experiments served as baselines to verify that the observed degradation was primarily attributable to photocatalytic mechanisms. Samples were withdrawn from the reactor at regular intervals and immediately filtered to isolate the catalyst. The residual concentration of SMZ was measured using a UV–Vis spectrophotometer by monitoring the absorbance at 278 nm, which is the characteristic peak for SMZ. For further confirmation and identification of intermediates, selected samples were analyzed using LC-MS. All experiments were carried out in triplicate to ensure reproducibility and average values were reported along with standard deviations. This comprehensive experimental design enabled a detailed understanding of the factors influencing SMZ degradation and provided insights into the efficacy of the N-doped $TiO_2/BC_{20\ \%}$ photocatalyst under varying conditions. The photocatalytic degradation experiments were conducted in a batch reactor system designed to ensure uniform mixing and controlled light exposure. The reactor was equipped with a magnetic stirrer to maintain a consistent reaction mixture and prevent the settling of the N-doped $TiO_2/BC_{20\ \%}$ nanocomposite. Illumination was provided by two light sources: a UV light source to activate the photocatalyst and natural sunlight to evaluate performance under real-world conditions. To block interference from ambient light during UV experiments, the reactor chamber was covered.

The concentration of SMZ during the photocatalytic degradation tests was primarily assessed using UV–Vis spectrophotometry. A UV–Vis spectrophotometer was set to measure absorbance at 278 nm, which corresponds to the maximum absorbance of SMZ. Calibration curves were prepared using standard SMZ solutions of known concentrations to ensure accuracy and linearity within the relevant concentration range. The residual concentration of SMZ in the reaction mixture at different time intervals was determined by comparing the absorbance of the samples with the calibration curve. This technique provided a rapid and reliable measure of SMZ degradation. To identify the degradation of intermediate byproducts formed during the photocatalytic reaction, LC-MS was employed. Samples were prepared by filtering out the catalyst and diluting the supernatant as needed. The LC-MS analysis was performed using a mobile phase of methanol and water, often in gradient elution mode, to ensure effective separation of byproducts. Mass spectrometric detection was conducted in positive ion mode, capturing the molecular ion peaks and fragment patterns of the intermediates. The identification of degradation products was based on their molecular weight and fragmentation profiles, allowing for a deeper understanding of SMZ degradation pathways. To evaluate the complete mineralization of SMZ, Total Organic Carbon (TOC) analysis was performed. TOC measurements quantified the reduction in organic carbon content in the reaction mixture, providing a direct indication of the conversion of organic matter to inorganic carbon. Samples were collected, filtered, and analyzed using a TOC analyzer [57]. The percentage reduction in TOC values reflected the degree of mineralization, offering a complementary metric to concentration-based degradation assessments. Together, these analytical methods provided a thorough assessment of SMZ degradation, the formation of intermediates, and the mineralization process, ensuring a comprehensive analysis of photocatalytic activity.

2.6. Optimization and data analysis

The experimental data collected during the photocatalytic degradation studies were analyzed using RSM, facilitated by the specialized software, Design-Expert. RSM allowed for the development of a predictive statistical model that clarifies the relationships between the experimental factors: pH, catalyst dosage, initial SMZ concentration, and contact time, along with the response variable, which was the percentage of SMZ degradation [58]. A quadratic polynomial model was employed to capture both linear and interactive effects among the factors, as well as any non-linear behavior. To evaluate the adequacy of the statistical model, key metrics such as R^2, adjusted R^2, and p-values for the model terms were analyzed [59]. The significance of factors and their interactions was assessed using analysis of variance (ANOVA), which also confirmed the model's reliability. Additionally, the degradation data were further analyzed to determine the reaction kinetics. The experimental results were fitted to a pseudo-first-order kinetic model, as expressed in Eq. (1).

$$ln\left(\frac{C_0}{C_t}\right) = kt \tag{1}$$

where C_0 is the initial concentration of SMZ, C_t is the concentration at time t, and k is the rate constant. The linearized form of the equation allowed the estimation of k from the slope of the plot of $\ln(C_0/C_t)$ versus time. The goodness-of-fit was evaluated using the correlation coefficient (R^2) and residual analysis.

The photocatalytic degradation process was optimized using desirability functions, which integrate various response variables into a single overall desirability score. An RSM-based model was employed to identify the optimal conditions for input factors such as SMZ concentration, pH, agitation time, and catalyst dosage, which enhanced degradation efficiency, as outlined in Table 1. Contour and surface plots were generated to illustrate the effects of these variables and their interactions. To validate the accuracy and predictive capability of the developed model, experimental runs were conducted under the predicted optimal conditions [60]. The degradation efficiencies observed from these experiments were assessed based on the optimal conditions. The percentage error and residuals were computed to evaluate the model's reliability, as indicated in Eq. (2). A strong agreement between the experimental results and predicted values confirmed the validity of the optimization process. This comprehensive data analysis approach provided a solid understanding of the photocatalytic degradation process, enabling effective optimization and validation of the experimental findings [61]. The reusability of the N-doped $TiO_2/BC_{20\ \%}$ nanocomposite was tested over six consecutive cycles to evaluate its performance and stability [62]. After each degradation experiment, the catalyst was recovered by filtration, thoroughly washed with deionized and/or distilled water to eliminate any residual contaminants, and dried at 105 °C. This dried nanocomposite was then reused under the same experimental parameters for subsequent cycles. The degradation efficiency of SMZ was monitored after each cycle to identify any reduction in photocatalytic activity, yielding insights into the catalyst's durability and suitability for repeated use. To examine the practical applicability of

Table 1
Factors and levels used in factorial design.

Levels	Factors	Levels		
		Low (−1)	Medium (0)	High (+1)
1	Time, (A)	30	75	120
2	Y	3	7	11
3	Dose, (C)	0.5	1.75	3
4	Initial Con. (D)	5	35	150

the optimized photocatalytic system, experiments were conducted using samples collected from real pharmaceutical industrial wastewater. These samples, representing complex environmental matrices, were treated under the same optimized conditions determined in the laboratory. The performance of the N-doped $TiO_2/BC_{20\ \%}$ nanocomposite in degrading SMZ and other potential pollutants present in the wastewater was evaluated, providing insights into the system's effectiveness in real-world applications.

$$Y = \beta_o + \sum_{i=1}^{k}\beta_i X_i + \sum_{i=1}^{k}\beta_{ii}X_i^2 + \sum_{i=1}^{k-1} * \sum_{j=2}^{k}\beta_{ij}X_i X_j + e_i \quad (2)$$

Where Y represents the dependent variable, which is the degradation efficiency. X_i and X_j denote the encoded independent variables. The coefficients β_0, β_i, β_{ii}, and β_{ij} stand for the linear, second-order, and interaction parameters in the regression model, respectively. K is the count of parameters involved, and e_i signifies the error term.

3. Results and discussion

3.1. wastewater characterization

The pharmaceutical wastewater collected from an industrial facility prior to treatment was carefully analyzed to evaluate its composition and contaminant levels. LC-MS analysis revealed a significant concentration of SMZ at 134.6 mg/L, indicating substantial pharmaceutical contamination. Key water quality parameters were also measured: the chemical oxygen demand (COD) was found to be 2498 mg/L, the biological oxygen demand (BOD) was 760 mg/L, and the TOC was 1050 mg/L. These figures highlight the high organic load and the persistent nature of the pollutants present. After undergoing photocatalytic treatment with the N-doped $TiO_2/BC_{20\ \%}$ nanocomposite, notable reductions in organic pollutants were observed. The removal efficiencies achieved were 93.2 % for COD, 90.1 % for BOD, and 92.7 % for TOC, demonstrating the catalyst's effectiveness in degrading pharmaceutical residues and decreasing overall organic contamination [32,33]. These findings support the potential of photocatalytic treatment as an advanced and sustainable method for managing pharmaceutical wastewater. For a more detailed understanding of the wastewater characteristics, including the presence of other pharmaceutical compounds, inorganic constituents, and potential toxic byproducts, please refer to our previous publication, which provides a comprehensive physicochemical characterization of the wastewater [50].

3.2. Characterization of nanocomposite

3.2.1. XRD analysis

This analysis confirms the coexistence of anatase and rutile phases within the synthesized nanocomposite, with anatase being the predominant phase. The prominent diffraction peaks observed at 25.3° (101), 37.8° (004), and 48.0° (200) are characteristic of the anatase structure, while smaller peaks at 27.5° (110), 36.09° (111), and 54.38° (211) correspond to the rutile phase, as shown in Fig. 1. This distribution indicates a mixed-phase TiO_2 material, which is often advantageous for catalytic applications due to the synergistic interactions between the phases [63]. Quantitative phase analysis reveals that the material comprises 12.6 % rutile and approximately 87 % anatase. After applying the material to pollutant degradation processes, significant changes were observed in the phase composition of the nanocomposite. The rutile content decreased from 12.6 % to 8.8 %, while the anatase phase increased from 87 % to 92 %. This shift can be attributed to the superior photocatalytic activity of anatase, which likely facilitated the transformation of the rutile phase under operational conditions [64]. The increased dominance of anatase after treatment supports its essential role in enhancing catalytic efficiency. A high anatase content is particularly beneficial, as it has been widely reported to exhibit greater activity in photocatalytic degradation due to its favorable bandgap and charge separation properties [65]. Although the presence of rutile decreased after treatment, it may have contributed to charge transfer processes that initially enhanced the degradation rate of organic pollutants. These phase transformations and their implications for the

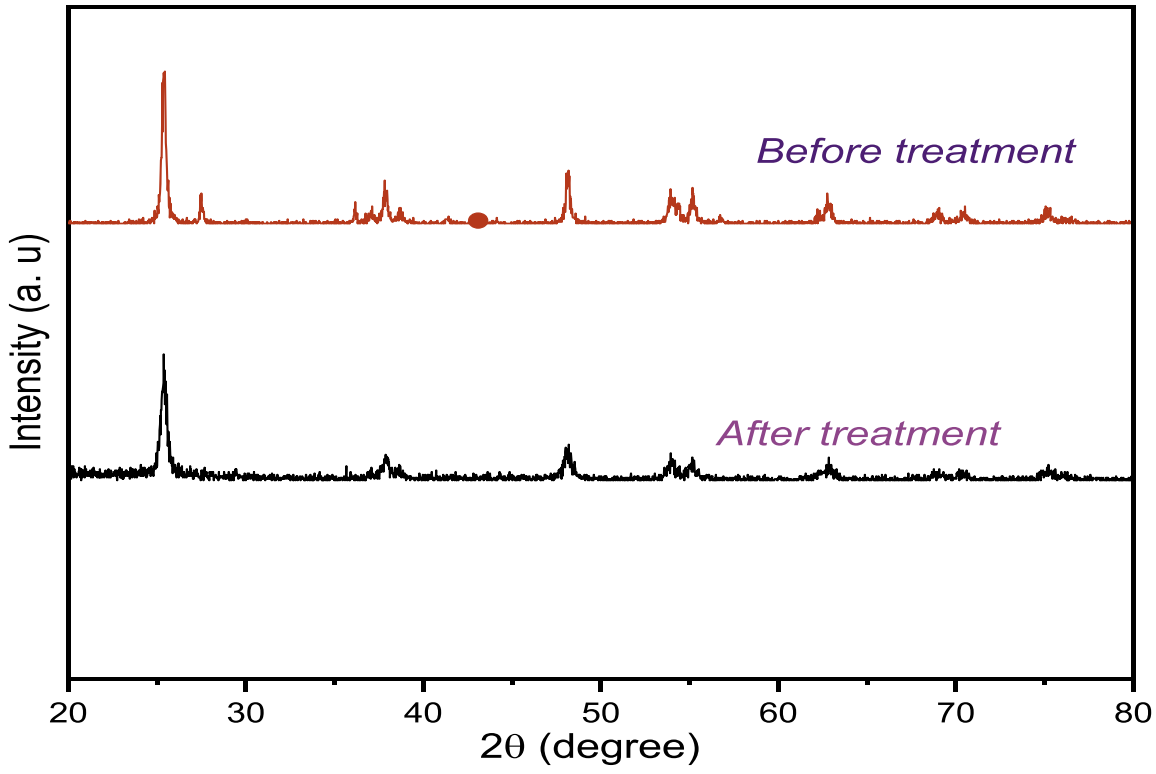


Fig. 1. XRD results before and after treatment of SMZ by N-doped $TiO_2/BC_{20\ \%}$ nanocomposite.

catalytic performance of the nanocomposite align with findings from previous studies, emphasizing the dynamic behavior of TiO_2 composites during environmental remediation applications.

3.2.2. SEM analysis

The SEM analysis was conducted to assess the surface morphology and distribution of TiO_2 on the BC substrate. The micrographs displayed in Fig. 2 clearly illustrate that the TiO_2 nanoparticles are uniformly dispersed across the BC surface. This even distribution ensures optimal contact between the active sites of TiO_2 and the surrounding environment, which is crucial for both catalytic and adsorption applications. Interestingly, the TiO_2 particles exhibit a spherical morphology, a hallmark of synthesized TiO_2 nanoparticles, consistent with findings reported in previous studies [66]. This spherical shape contributes to an increased surface area, facilitating effective interactions with target pollutants an essential factor in enhancing photocatalytic activity and adsorption efficiency [67]. The integration of TiO_2 and BC within a composite material is vital for the degradation of pollutants. Biochar offers a high surface area and a porous structure, providing a supportive matrix for TiO_2, while the well-dispersed TiO_2 further enhances the composite's photocatalytic properties. This synergistic configuration increases the likelihood of pollutant molecules adsorbing onto the catalyst's surface [68]. In summary, the SEM analysis results confirm the successful synthesis of the N-doped $TiO_2/BC_{20\ \%}$ nanocomposite, exhibiting the desired structural and morphological characteristics. The uniform distribution and spherical shape of the TiO_2 nanoparticles on biochar underscore the material's potential for advanced contaminant degradation and adsorption processes.

The elemental composition of N-doped $TiO_2/BC_{20\ \%}$ nanocomposite was analyzed using energy-dispersive X-ray spectroscopy (EDS) and presented in Fig. 3. The EDS results indicate the presence of Carbon (15 %), Oxygen (36 %), and Titanium (47 %). However, N, which was incorporated as a dopant during nanocomposite synthesis, was not detected in the spectrum of N-$TiO_2/BC_{20\ \%}$. The absence of N in EDS results for the N-doped $TiO_2/BC_{20\ \%}$ nanocomposite aligns with similar observations reported in previous literature. EDS has limited sensitivity for detecting light elements like N, particularly when present in trace amounts or embedded within a matrix dominated by heavier elements such as titanium [69]. Nitrogen doping often occurs in substitutional or interstitial forms within the TiO_2 lattice, which may not produce distinct chemical phases detectable by EDS. Moreover, the overlap of nitrogen's X-ray emission lines with those of other light elements, such as carbon, can mask its signal. Studies by Zhang et al. and Kumar et al. have shown that, despite nitrogen doping, EDS may fail to detect nitrogen due to these intrinsic limitations [70,71]. Instead, complementary techniques like X-ray Photoelectron Spectroscopy (XPS) or FTIR are recommended for confirming nitrogen incorporation. However, the FTIR result confirms the presence of N-doped TiO_2 is evident from the 729.6 cm^{-1} peak, which likely arises from N–Ti–O vibrations, confirming successful nitrogen incorporation into the TiO_2 lattice. In addition, peak 1581.12 cm^{-1} is most probably indicative of the existence of N–H bending or Ti–N stretching, further supporting nitrogen doping [72]. Another plausible explanation is the potential loss of nitrogen during the synthesis or analysis process. High-temperature synthesis conditions, often employed in creating N-doped TiO_2, can cause nitrogen volatilization, reducing its detectable content in the final material. Despite the absence of a detectable nitrogen signal, the doped nitrogen can still influence the composite's properties, such as modifying its bandgap or improving photocatalytic activity, as noted in studies by [73]. These indirect effects highlight that N-doping may not always be evident in elemental analysis but can be inferred from changes in the material's functional performance. Future investigations should integrate advanced characterization methods like XPS and UV–Vis spectroscopy to confirm N-doping and assess its impact on the composite's structure and behavior.

3.2.3. FTIR analysis

This confirms the presence of several significant functional groups within the N-doped $TiO_2/BC_{20\ \%}$ nanocomposite, as illustrated in Fig. 4. These functional groups are crucial for understanding the structural and chemical interactions in the composite material. The peak at 442 cm^{-1} corresponds to the Ti–O–Ti bending vibration, a characteristic feature of the anatase phase of TiO_2, indicative of its crystalline structure [74]. Similarly, the peak at 638.39 cm^{-1} is attributed to Ti–O stretching or bridging oxygen vibrations, commonly observed in the TiO_2 lattice [75]. The presence of N-doped TiO_2 is evident from the 729.6 cm^{-1} peak, which likely arises from N–Ti–O vibrations, confirming successful nitrogen incorporation into the TiO_2 lattice. Alternatively, this peak might also suggest the presence of $C = N$ bonds in the biochar matrix, contributing to enhanced interaction between the TiO_2 and biochar phases. Other prominent peaks highlight interactions between the biochar and TiO_2. The peak at 1182.23 cm^{-1} is associated with C–O stretching vibrations, which could also represent Ti–O–C bonds, implying strong coupling between biochar and TiO_2 [76]. The 1581.12 cm^{-1} peak is indicative of $C = C$ stretching in aromatic structures,

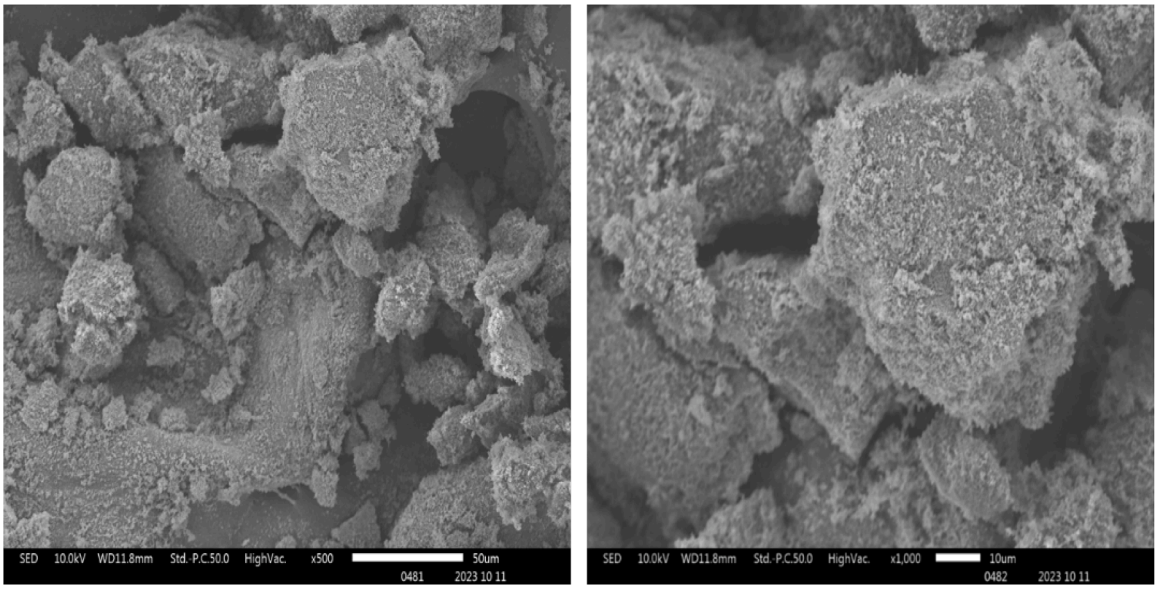


Fig. 2. SEM results of N-doped $TiO_2/BC_{20\ \%}$ nanocomposite at 50 and 100 μm.

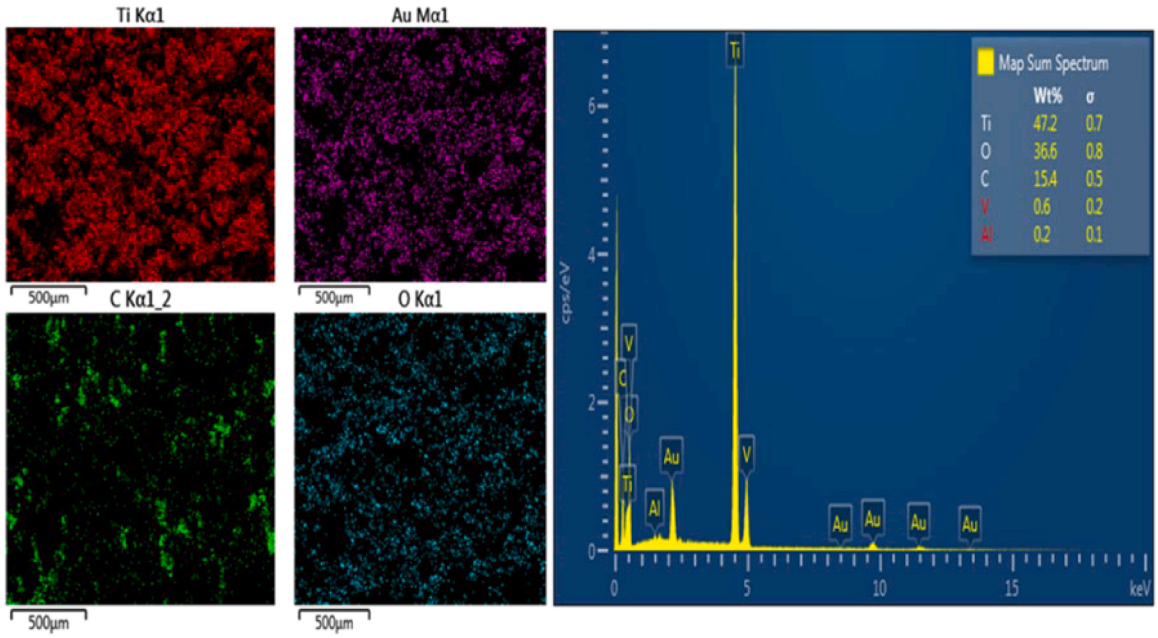


Fig. 3. EDS results of N-doped $TiO_2/BC_{20\ \%}$ nanocomposite.

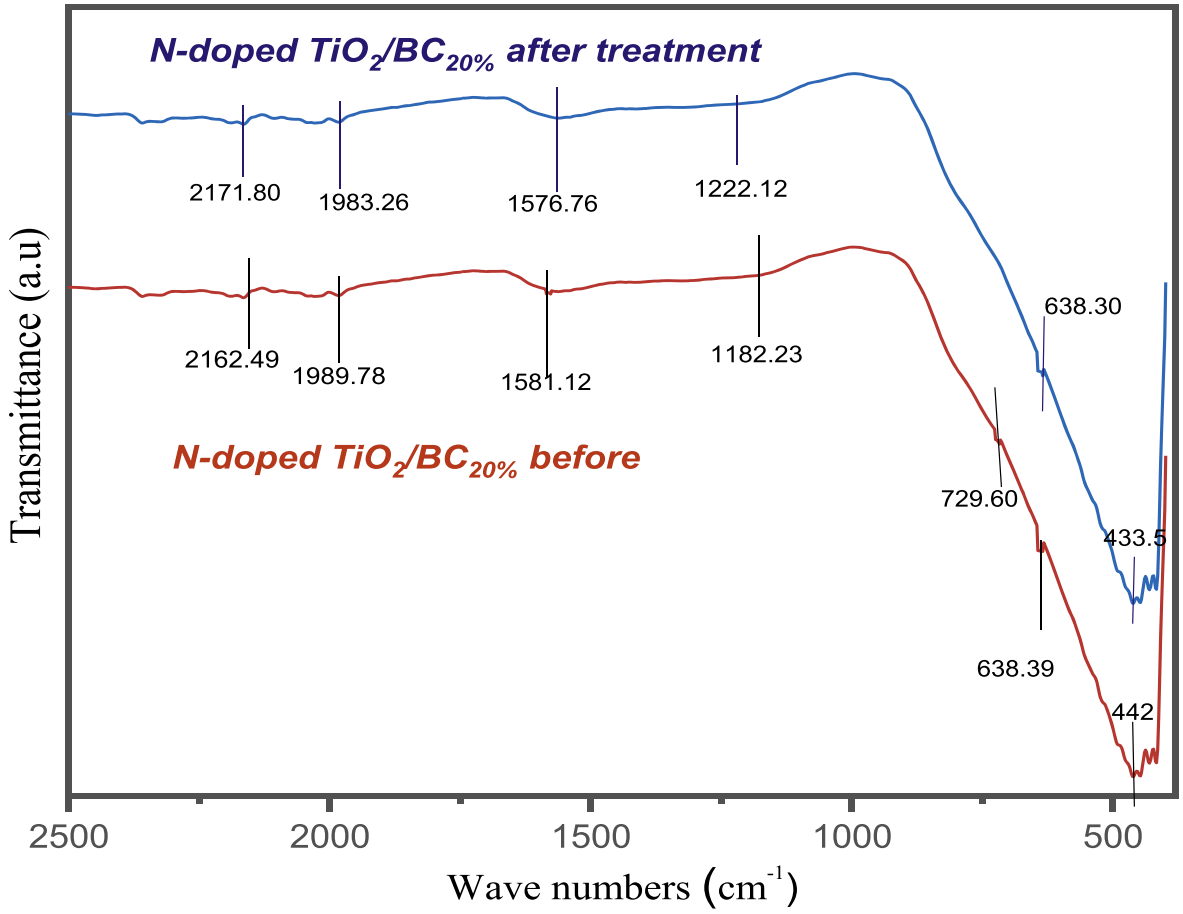


Fig. 4. FTIR results of N-doped $TiO_2/BC_{20\ \%}$ nanocomposite before and after treatment.

reflecting the biochar's graphitic framework, or it could be related to N–H bending or Ti–N stretching, further supporting nitrogen doping [72]. Additionally, the high-energy peak at 1989 cm^{-1} is likely an overtone or combination band associated with TiO_2 vibrations or surface interactions. The 2162 cm^{-1} peak suggests the presence of C≡N stretching vibrations, which are indicative of nitrile groups, or possibly isocyanate (–*N* = *C* = *O*) functionalities that arise from nitrogen incorporation. The FTIR spectra after five application cycles reveal that most

functional groups persist, albeit with slight shifts in peak positions. Peaks were observed at 433.5, 638.3, 1222.12, 1576.76, 1983.26, and 2171.8 cm^{-1}, confirming the structural stability of the composite material under repeated usage. However, the peak at 729.6 cm^{-1} disappears, suggesting a possible degradation or modification of the N–Ti–O or *C = N* functional group during repeated applications [28]. This indicates that while the nanocomposite retains its core structural features, specific interactions might weaken or transform under prolonged use. These observations align with existing studies on N-doped TiO_2 and biochar composites, which highlight the role of functional groups in enhancing material properties such as photocatalytic activity and chemical stability [77]. The retention of key functional groups after repeated use underscores the durability of the composite, while the minor structural changes suggest areas for further optimization in future applications.

3.2.4. Point zero charge

The photocatalytic degradation performance of N-doped $TiO_2/BC_{20\ \%}$ nanocomposite in the degradation of SMZ is significantly influenced by the pH of the solution. This pH affects the surface charges of the catalyst and the ionization state of SMZ. The point of zero charge (pH_pzc) for the nanocomposite is 5.7, indicating that the surface is positively charged at pH levels below this value and negatively charged at pH levels above it, as shown in Fig. 5. SMZ has pKa values of approximately 1.7 and 5.6, which means it transitions from a cationic state at very low pH to a neutral form near pH 5.6, before becoming anionic at higher pH values [78]. The maximum removal efficiency occurs at pH 5 because, at this level, the neutral SMZ molecules dominate and the photocatalyst is nearly neutral. At this pH, electrostatic repulsion is minimal, leading to better adsorption of SMZ onto the catalyst surface, which enhances photocatalytic degradation. Neutral SMZ has been found to interact more strongly with photocatalysts and to be more susceptible to degradation when exposed to UV light or sunlight [79]. At pH levels below 5, the positively charged surface interacts less favorably with the neutral or cationic forms of SMZ, resulting in decreased adsorption efficiency. Conversely, at pH levels above 5.7, the negatively charged surface of the catalyst experiences electrostatic repulsion with the anionic form of SMZ, thereby reducing removal efficiency. These findings align with previous studies that highlight the importance of pH in governing adsorption and photocatalytic processes [80]. The results are consistent with the understanding that slightly acidic to near-neutral pH conditions often yield optimal performance for the photocatalytic removal of pharmaceuticals. Research on the degradation of SMZ has emphasized the crucial role of pH in modulating interactions between the compound and various photocatalysts, confirming that neutral and non-repulsive states enhance overall efficiency [81]. In summary, the interaction between the pH_pzc of the N-doped $TiO_2/BC_{20\ \%}$ nanocomposites and the pKa values of SMZ determines the optimal conditions for its degradation. Maintaining a solution pH of around 5 ensures favorable adsorption dynamics and efficient photocatalytic activity, leading to superior removal outcomes.

3.3. Optimization of photocatalysis

The study involved a central composite design for the photocatalytic degradation of SMZ, utilizing Response RSM software for model fitting and statistical analysis, as detailed in Table 2. The experimental design included four main influencing factors and six central points across a total of 30 runs. The suitability of quadratic modeling was evaluated using analysis of variance (ANOVA). The results from RSM showed that the input response variables had significant parameters (p-value $<$ 0.001). The model's statistical relevance was confirmed by a calculated F-value of 4765.03, which corresponded to a highly significant p-value ($<$0.0001). The model demonstrated a strong fit to the data, as indicated by a high R^2 value of 0.9998, further supported by an adjusted R^2 value of 0.9996. Additionally, the model's validity was confirmed by a non-significant lack of fit (p-value = 0.3014), which exceeded the 0.05 significance threshold. Table 3 summarizes the results from the four-factor central composite design studies on SMZ degradation. The degradation efficiency observed was close to the predicted value of 98.6 %, compared to 98.3 % recorded for the actual run. Regression equations and quadratic models generated using specialized software were employed to analyze the experimental data. These equations illustrate the relationship between the coded and actual variables for SMZ degradation percentage in both coded and exact forms. In this study, degradation efficiency was optimized using N-doped $TiO_2BC_{20\ \%}$. The software was used to assess the effects of selected parameters, such as agitation time, pH, nanocomposite dosage, and the initial concentration of SMZ, as well as their interactions, to establish optimal conditions for achieving maximum degradation efficiency [82]. Eq. (3) reflects the relationships between the independent variable (degradation efficiency) and the other five dependent variables. This equation is crucial for evaluating significant operational parameters, their interactions, and

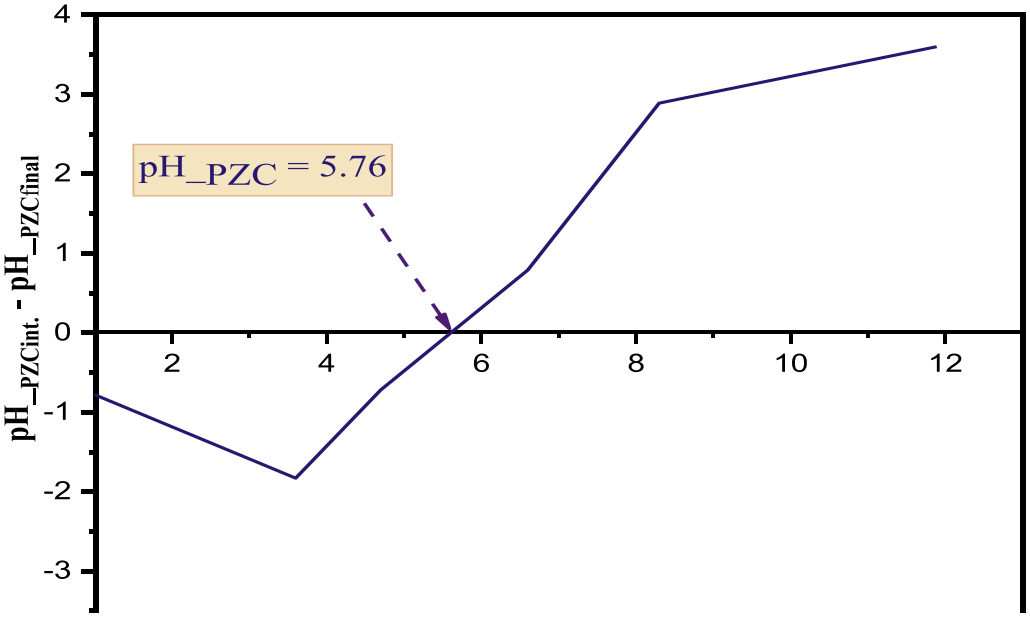


Fig. 5. Point zero charge of N-doped $TiO_2/BC_{20\ \%}$ nanocomposite.

Table 2
Experimental data points and responses used in the CCD.

Std	Run	pH	Time	Initial Conc.	Dose	SMZ degradation	Predicted Degradation
			Min	mg/L	g/L	%	%
20	1	7	120	75	2.5	84.99	84.90
11	2	5	95	40	3.5	92.22	92.23
7	3	5	95	110	1.5	97.39	97.49
4	4	9	95	40	1.5	75.55	75.42
12	5	9	95	40	3.5	68.23	68.26
21	6	7	70	5	2.5	89.55	89.50
3	7	5	95	40	1.5	98.34	98.57
6	8	9	45	110	1.5	85.09	84.95
28	9	7	70	75	2.5	79.55	79.62
5	10	5	45	110	1.5	93.02	92.93
9	11	5	45	40	3.5	94.388	94.33
22	12	7	70	145	2.5	93.01	93.25
30	13	7	70	75	2.5	79.67	79.62
23	14	7	70	75	0.5	95.11	94.99
17	15	3	70	75	2.5	93.89	93.58
14	16	9	45	110	3.5	83.2	82.91
13	17	5	45	110	3.5	91.73	91.73
19	18	7	20	75	2.5	89.89	90.17
2	19	9	45	40	1.5	82.52	82.41
25	20	7	70	75	2.5	79.77	79.62
8	21	9	95	110	1.5	81.78	81.78
27	22	7	70	75	2.5	79.65	79.62
29	23	7	70	75	2.5	79.72	79.62
15	24	5	95	110	3.5	93.39	93.44
16	25	9	95	110	3.5	77.21	76.90
1	26	5	45	40	1.5	97.65	97.83
10	27	9	45	40	3.5	78.32	78.08
24	28	7	70	75	4.5	86.31	86.62
26	29	7	70	75	2.5	79.34	79.62
18	30	11	70	75	2.5	61.12	61.62

predicting SMZ degradation efficiency under various operational conditions.

$$SMZ\ (RE\ \%) = 79.62 - 7.89A - 1.32B + 0.93C - 2.09D - 1.93AB + 1.83AC - 0.71AD + 0.95BC - 0.71BD + 0.57CD - 0.38A^2 + 1.96B^2 + 2.92C^2 + 2.77D^2 \quad (3)$$

Where the coded symbols represent A for contact time, B for pH, C for catalyst dose, and D for the initial concentration of SMZ

A comprehensive residual analysis was carried out to evaluate the effectiveness and appropriateness of the model developed for the degradation of SMZ using the N-doped $TiO_2/BC_{20\ \%}$ nanocomposite. This analysis involved two key components: the predicted versus actual values plot and the normal probability plot of the residuals. The normal probability plot was utilized to assess whether the residuals, essentially the differences between the observed values and the predicted values, followed a normal distribution. This is an important aspect of regression analysis as it impacts the validity of the statistical inferences made from the model. As illustrated in Fig. 6, the plot displayed a straight-line pattern, which is indicative of a normal distribution of the residuals. This observation not only supports the model's underlying assumptions but also enhances the credibility of the overall results obtained from the analysis. In addition to the normal probability plot, a thorough examination of the predicted versus actual values plot was conducted. This plot serves a critical role in gauging the model's predictive accuracy by allowing for a direct comparison between the experimental results and the values predicted by the model. The close alignment of the predicted data with the observed data, as evidenced by their proximity along the diagonal line of the plot, underscores the model's precision and reliability. Taken together, these analyses provide strong evidence that the model is a robust fit for the experimental data [83]. Furthermore, the results affirm that it adheres to the critical assumptions necessary for ensuring reliable predictions in RSM. Overall, this rigorous assessment enhances our confidence in the model's capability to accurately predict the degradation of SMZ, reinforcing its practical applicability in relevant environmental science contexts.

The evaluation of DFFITS in comparison to RUN for the N-doped TiO_2/BC nanocomposite in the degradation of SMZ indicated that the majority of data points fell within the designated boundary, suggesting that most model runs conformed to acceptable limits. However, a few points were identified outside this boundary, indicating that these specific runs could exert a greater influence on the model's behavior. As illustrated in Fig. 7, this trend highlights the overall robustness of the model while also drawing attention to particular runs that may affect its reliability and stability. These findings are crucial for understanding the impact of individual data points on the model's performance.

As illustrated in Fig. 8, a remarkable removal efficiency of 98.34 % was achieved during the RSM optimization process under specific conditions. The optimal parameters identified in this study included an

Table 3
ANOVA of the quadratic model of photodegradation of SMZ by N-doped $TiO_2/BC_{20\ \%}$.

Source	Sum of Squares	df	Mean Square	F-value	p-value	
Model	2282.44	14	163.03	4765.03	< 0.0001	significant
A-pH	1494.81	1	1494.81	43,689.81	< 0.0001	
B-Time	41.63	1	41.63	1216.68	< 0.0001	
C-Initial Conc.	21.12	1	21.12	617.18	< 0.0001	
D-Dose	105.22	1	105.22	3075.32	< 0.0001	
AB	59.72	1	59.72	1745.54	< 0.0001	
AC	55.23	1	55.23	1614.38	< 0.0001	
AD	0.6839	1	0.6839	19.99	0.0004	
BC	14.57	1	14.57	425.83	< 0.0001	
BD	8.08	1	8.08	236.07	< 0.0001	
CD	5.23	1	5.23	153.01	< 0.0001	
A^2	3.99	1	3.99	116.47	< 0.0001	
B^2	104.84	1	104.84	3064.28	< 0.0001	
C^2	233.08	1	233.08	6812.40	< 0.0001	
D^2	210.85	1	210.85	6162.64	< 0.0001	
Residual	0.5132	15	0.0342			
Lack of Fit	0.3941	10	0.0394	1.65	0.3014	not significant
Pure Error	0.1191	5	0.0238			
Cor Total	2282.95	29				
Statistical Fit Summary of Degradation						
Source	Std. Dev.	R^2	Adjusted R^2	Predicted R^2	Press	
Linear	4.98	0.7283	0.6849	0.6192	869.28	
2FI	5.01	0.7912	0.6813	0.6585	779.62	
Quadratic	0.1850	0.9998	0.9996	0.9989	2.44	Suggested

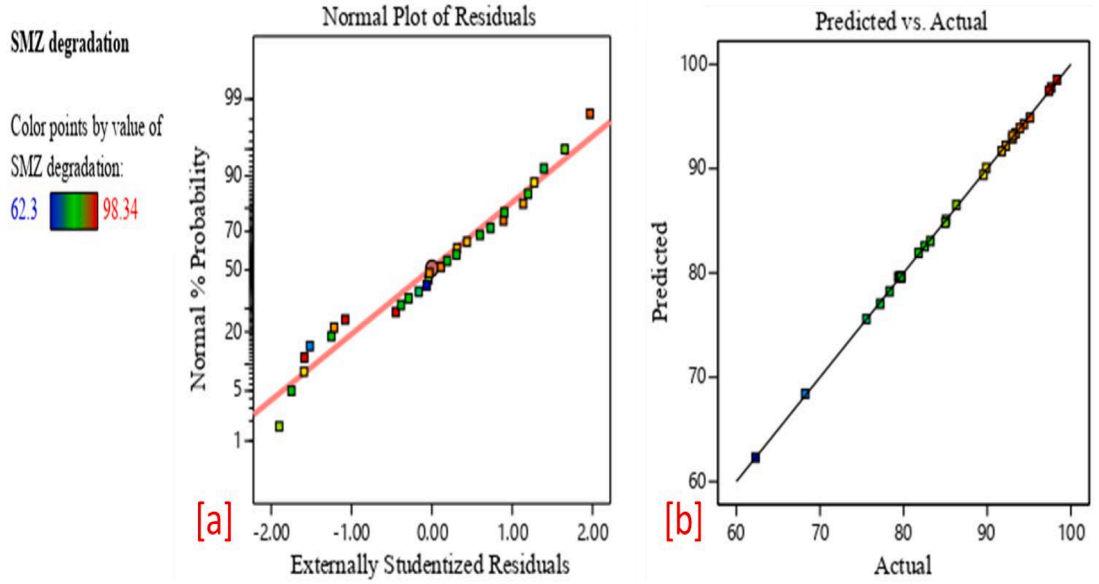


Fig. 6. [a] Normal plot of residual and [b] Actual Vs. predicted value of N-doped $TiO_2/BC_{20\ \%}$ nanocomposite.

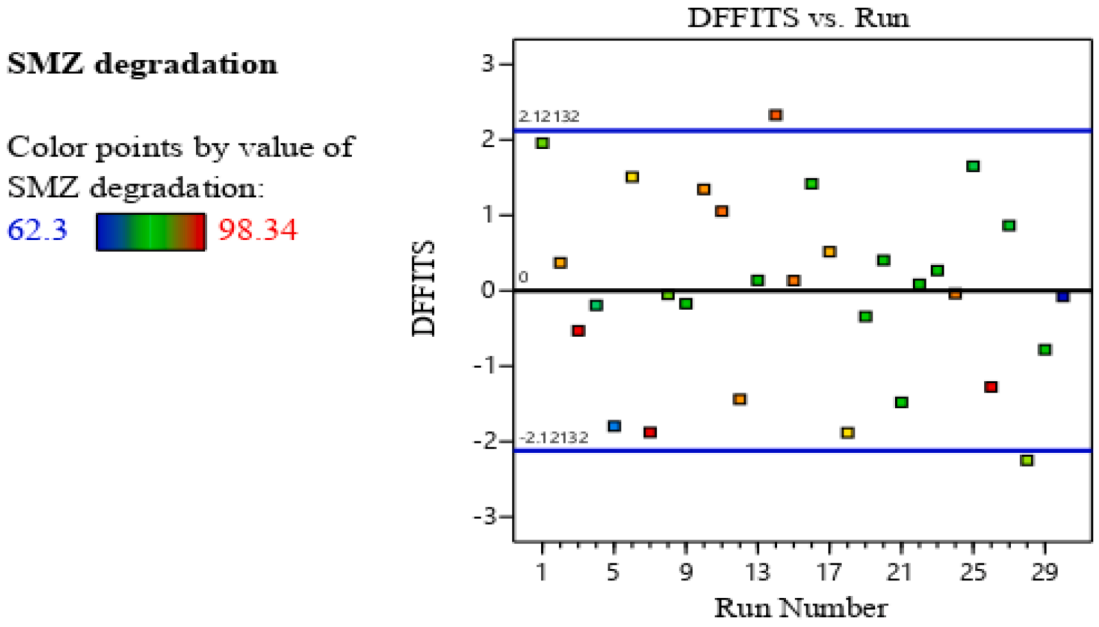


Fig. 7. Graphic representation of DFFITS vs. Run for by N-doped $TiO_2/BC_{20\ \%}$ nanocomposite.

agitation time of 95 min, a pH level of 5, a nanocomposite dosage of 1.5 g/L, and an SMZ concentration of 110 mg/L. These results underscore the efficacy of RSM in optimizing complex processes by systematically fine-tuning multiple variables to identify the ideal conditions for maximum performance. The application of RSM enhances our understanding of the interactions among various factors, which is essential for improving contaminant removal efficiency.

3.4. The interaction effects of photocatalysis's parameters

Effect of Time and pH: The optimization of photocatalytic degradation of SMZ in real pharmaceutical industry wastewater utilizing N-doped $TiO_2/BC_{20\ \%}$ was systematically examined through factorial design and RSM. The degradation efficiency was significantly influenced by pH levels, with optimal degradation observed at approximately pH 5, as illustrated in Fig. 9 during the optimization process. This observation is consistent with previous studies indicating that acidic conditions enhance the photocatalytic activity of TiO_2-based materials. This enhancement is attributed to increased protonation of the catalyst surface, which facilitates the adsorption of organic pollutants [84]. In contrast, as pH increased from 5 to 9, the removal efficiency markedly decreased. This decline can be attributed to a reduction in the availability of •OH, which is crucial for the oxidation of SMZ, as well as the likely interference with the pollutant's adsorption onto the catalyst surface due to ionization at higher pH levels [85,86]. Moreover, degradation efficiency showed a positive correlation with agitation time; extended exposure to UV light resulted in greater generation of electron-hole pairs in the N-doped $TiO_2/BC_{20\ \%}$ system, thus producing more reactive species for SMZ degradation [87]. The factorial design revealed a significant interaction between pH and agitation time, indicating that optimal conditions rely not only on individual factors but also on their combined effects. Therefore, maintaining a slightly acidic

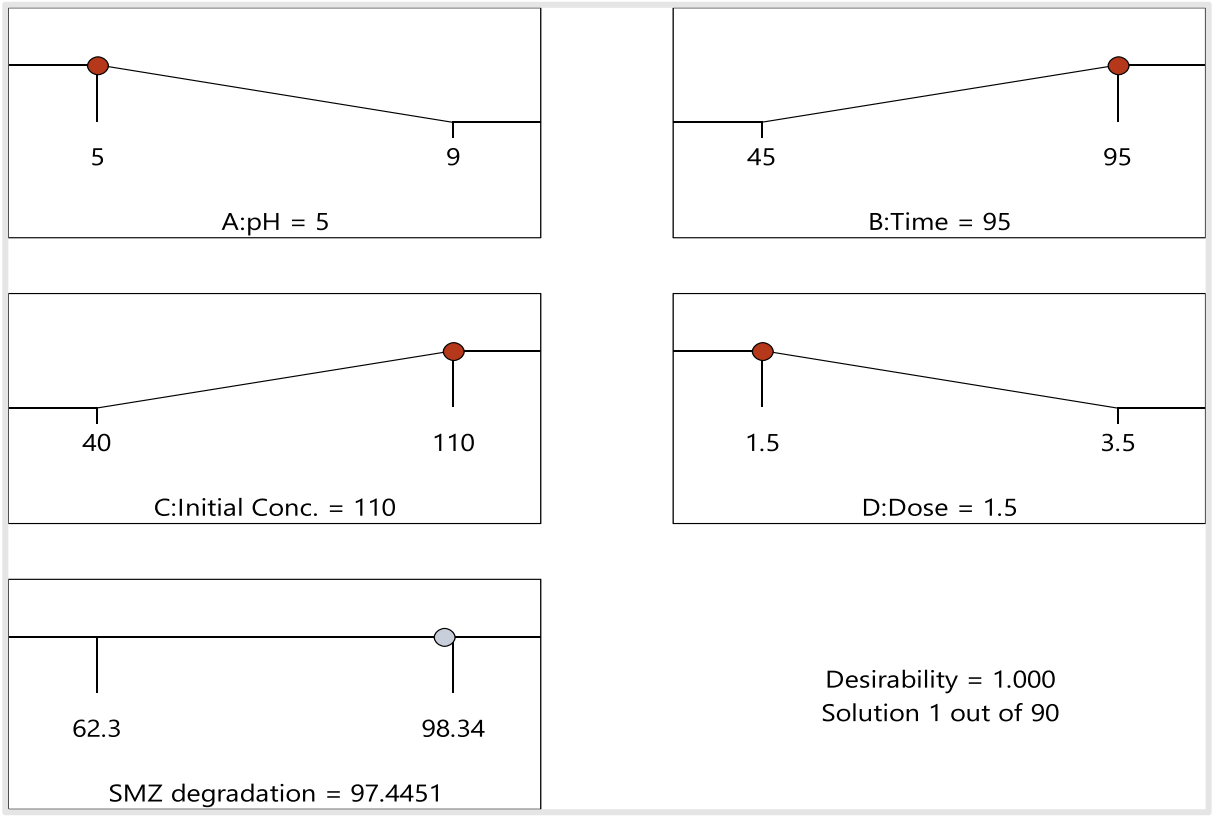


Fig. 8. Process Optimization of the degradation process under various parametric conditions against SMZ by N-doped $TiO_2/BC_{20\ \%}$ nanocomposite.

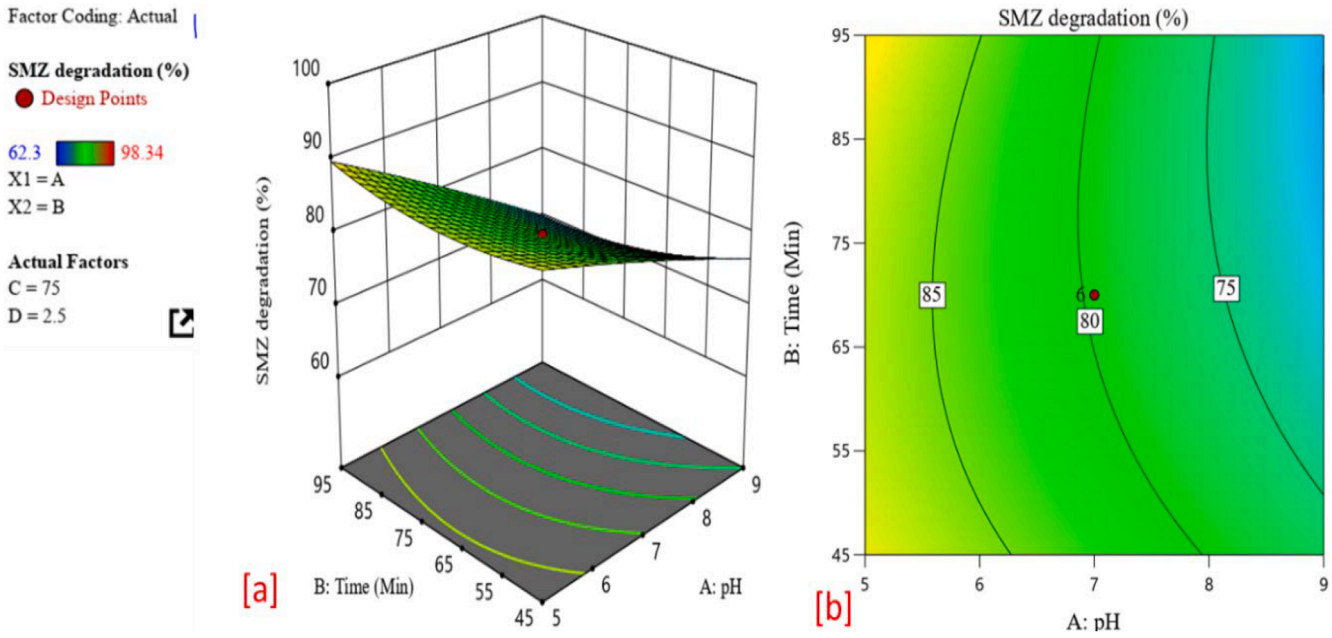


Fig. 9. [a] the 3D response surface, and [b] contour map showing the interaction of contact time and pH.

condition (pH 5) while extending reaction time can maximize degradation efficiency. These findings highlight the necessity of concurrently optimizing multiple parameters in photocatalytic processes and suggest avenues for future research, particularly focusing on the underlying mechanisms of these interactions and the potential for scaling this technology for practical wastewater treatment applications.

***Effects of Initial Concentration and* pH:** The optimization of photocatalytic degradation of sulfonamide antibiotics (SMZ) in actual pharmaceutical industry wastewater using N-doped $TiO_2/BC_{20\ \%}$ was thoroughly analyzed through factorial design and RSM. The results indicated that the removal efficiencies of the target pollutants were significantly influenced by pH and initial concentration, as shown in Fig. 10. Specifically, degradation rates improved at lower values of both parameters, with optimal degradation occurring at a pH of

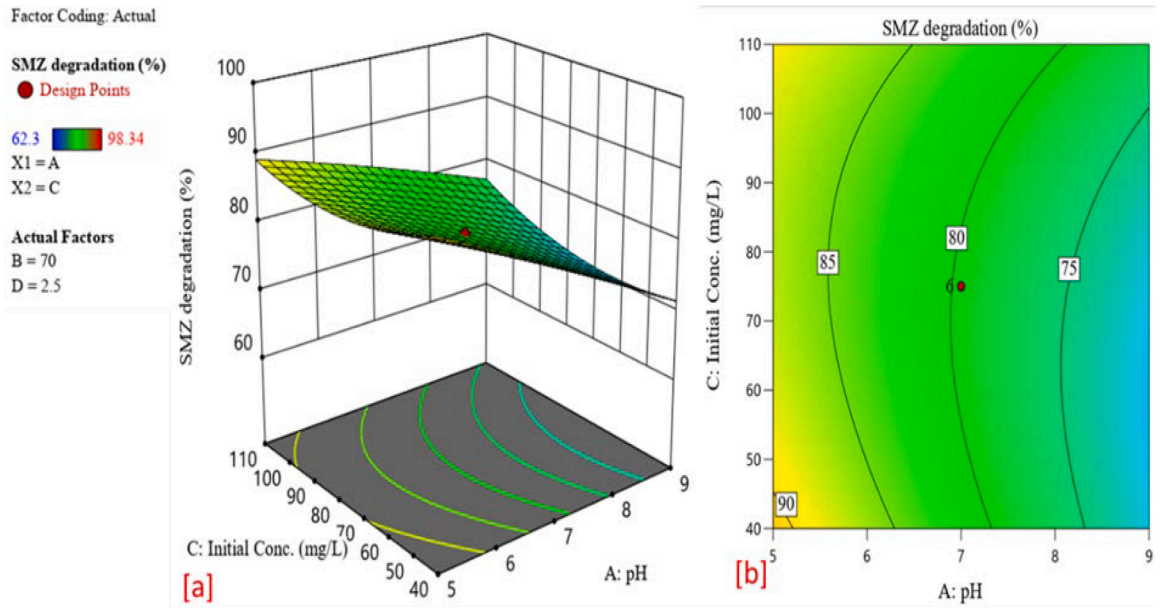


Fig. 10. [a] the 3D response surface, and [b] 2D contour map showing the interaction of initial concentration and pH.

approximately 5 and an initial concentration of around 40 mg/L. This trend can be attributed to the enhanced adsorption of SMZ onto the N-doped $TiO_2/BC_{20\ \%}$ surface under slightly acidic conditions, which facilitates the generation of reactive species essential for effective photocatalysis [88]. However, as pH increased from 5 to 9, a slight decrease in degradation efficiency was observed. This decline may be due to the reduced presence of hydroxyl radicals (•OH) at elevated pH levels, which are crucial for oxidizing SMZ. Additionally, there may be a reduction in antibiotic adsorption due to its ionization at higher pH levels. Similarly, increasing the initial concentration of SMZ from 40 to 110 mg/L resulted in decreased degradation efficiency. At higher concentrations, the availability of active sites on the photocatalyst becomes limited, leading to saturation effects where not all SMZ molecules can be effectively degraded [55]. This phenomenon aligns with findings from other studies that emphasize the importance of optimizing both pH and initial concentration to achieve maximum photocatalytic activity. The interaction between pH and initial concentration underscores the necessity of a balanced approach in photocatalytic processes, where both parameters must be carefully controlled to enhance degradation efficiency. Overall, these results highlight the potential of N-doped $TiO_2/BC_{20\ \%}$ as an effective photocatalyst for removing SMZ from pharmaceutical wastewater while indicating the need for further research to explore the underlying mechanisms and optimize operational conditions for practical applications.

***The Effects of Dose and* pH**: This study examined the optimization of photocatalytic degradation of SMZ in actual pharmaceutical wastewater using N-doped $TiO_2/BC_{20\ \%}$. The focus was on the interaction effects of pH and the dosage of the nanocomposite. The findings revealed that degradation efficiency improved at lower values for both parameters, with optimal degradation observed at a pH of approximately 5 and a nanocomposite dosage of around 2.5 g/L, as illustrated in Fig. 11. This enhancement is attributed to the favorable adsorption of SMZ onto the surface of N-doped $TiO_2/BC_{20\ \%}$, influenced by the pH_pzc of the nanocomposite and the pKa value of the solution. At pH levels below pH_pzc, the surface of the nanocomposite acquires a positive charge, facilitating the adsorption of negatively charged SMZ anions [84].

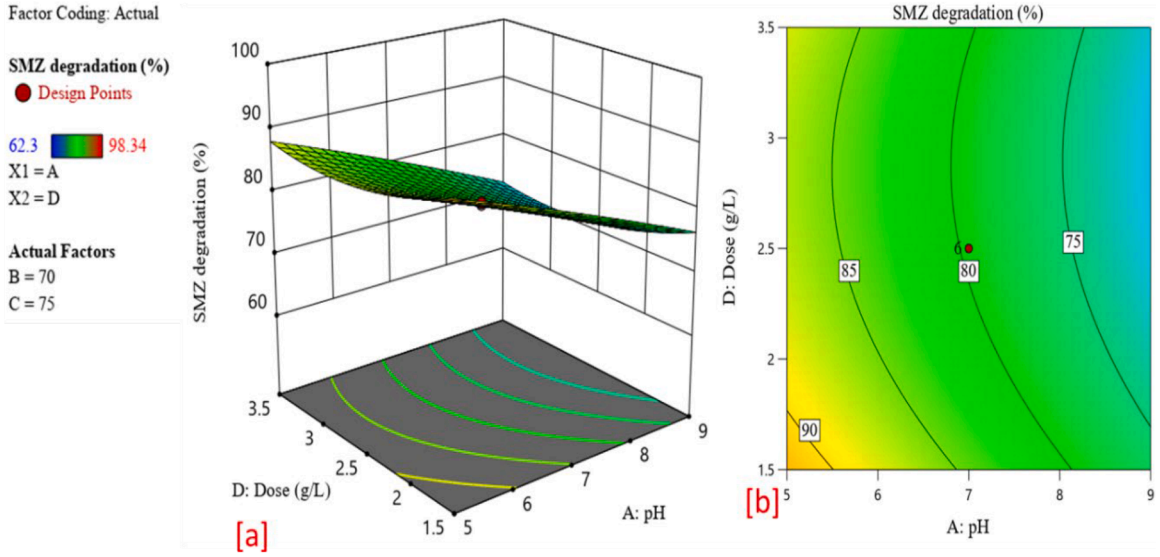


Fig. 11. [a] the 3D response surface, and [b] contour map showing the interaction of catalyst dose and pH.

Furthermore, while increasing the nanocomposite dosage beyond 2.5 g/L initially boosts degradation, a slight decrease in efficiency is observed at higher concentrations. This decline can be explained by light shielding effects, where an excess of the nanocomposite obstructs UV light from adequately penetrating the solution, thereby limiting photocatalytic activity [89]. This phenomenon underscores the necessity of optimizing photocatalyst dosage to strike a balance between providing a sufficient surface area for adsorption and ensuring adequate light penetration for photocatalytic reactions [90]. Overall, these results underscore the significant impact of both pH and nanocomposite dosage in optimizing the photocatalytic degradation of SMZ, highlighting the importance of carefully regulating these factors to enhance wastewater treatment efficiency.

The Effects of Initial Concentration and Time: The optimization of photocatalytic degradation of SMZ in real pharmaceutical wastewater using N-doped $TiO_2/BC_{20\ \%}$ was evaluated based on the initial concentration of SMZ and contact time. The results indicated that degradation efficiency improved with longer contact times, showing a direct relationship between exposure duration and the effectiveness of the photocatalytic process, as illustrated in Fig. 12. This enhancement can be attributed to the extended interaction time between SMZ and the reactive species produced during photocatalysis, such as •OH and superoxide anions ($\bullet O^{2-}$). As contact time increases, more radicals are generated in the solution, facilitating the breakdown of SMZ molecules and leading to higher degradation rates [72]. On the other hand, the relationship between degradation efficiency and the initial concentration of SMZ revealed a more complex interaction. While lower concentrations of SMZ allowed for effective degradation, higher initial concentrations resulted in a slight decrease in degradation efficiency. This decrease can be explained by the saturation effect; as pollutant concentrations rise, more SMZ molecules compete for active sites on the surface of the photocatalyst [91]. Furthermore, at elevated concentrations, the presence of additional SMZ molecules can hinder light penetration due to light shielding effects [55,92]. In this scenario, excess molecules absorb or scatter the incident light, reducing the intensity of light that reaches the photocatalyst. This reduction in light availability limits the excitation of electron-hole pairs in the photocatalyst, which are essential for generating the reactive species needed for degradation. Overall, these findings highlight the importance of optimizing both contact time and initial concentration in photocatalytic processes [93]. While longer contact times generally enhance degradation efficiency, excessively high initial concentrations can impede the effectiveness of the photocatalytic system. Future studies should focus on identifying the optimal balance between these parameters to maximize the degradation of SMZ in wastewater treatment applications.

The Effect of Time and Dose: Optimization of Photocatalytic Degradation of SMZ in Real Pharmaceutical Industry Wastewater Using N-Doped $TiO_2/BC_{20\ \%}$. The study analyzed the impact of nanocomposite dosage and contact time on the photocatalytic degradation of SMZ. The results indicated that the degradation efficiency decreased as the dosage of the nanocomposite increased, as shown in Fig. 13. This decline is attributed to the phenomenon known as light shielding, which occurs when an excessive amount of photocatalyst particles in the solution obstructs the light needed to activate the photocatalytic process. As the dosage of N-doped $TiO_2/BC_{20\ \%}$ increases, the particles may aggregate and scatter light, reducing the effective intensity of light reaching the photocatalyst. This, in turn, limits the generation of reactive species, such as •OH, which are crucial for the degradation of SMZ [92,94]. Conversely, the degradation efficiency showed a positive correlation with contact time. As contact time increased, the chances of interaction between SMZ molecules and the reactive radicals produced by the photocatalyst also increased. This longer interaction period enables more effective degradation of SMZ, as the radicals have more opportunities to react with and break down the pollutant molecules [90]. The combination of extended contact time and the presence of reactive radicals enhance the overall degradation process, highlighting the importance of optimizing both factors in photocatalytic applications. These findings suggest that, although increasing the nanocomposite dosage may initially appear beneficial, it is vital to consider the potential negative effects of light shielding [95]. Therefore, a careful balance must be maintained between the amount of photocatalyst used and the duration of contact time to maximize the degradation efficiency of SMZ in pharmaceutical wastewater treatment processes.

The Effect of Dose and Initial Concentration: The Effect of Dose and Initial Concentration: The optimization of photocatalytic degradation of SMZ in real pharmaceutical wastewater using N-doped $TiO_2/BC_{20\ \%}$ was studied with respect to the dosage of the nanocomposite and the initial concentration of SMZ. The findings revealed that degradation efficiency decreased as the amount of N-doped $TiO_2/BC_{20\ \%}$ nanocomposite increased, as illustrated in Fig. 14. This reduction can be attributed to light shielding effects, where higher concentrations of photocatalyst particles obstruct light penetration into the solution. As the dosage of the

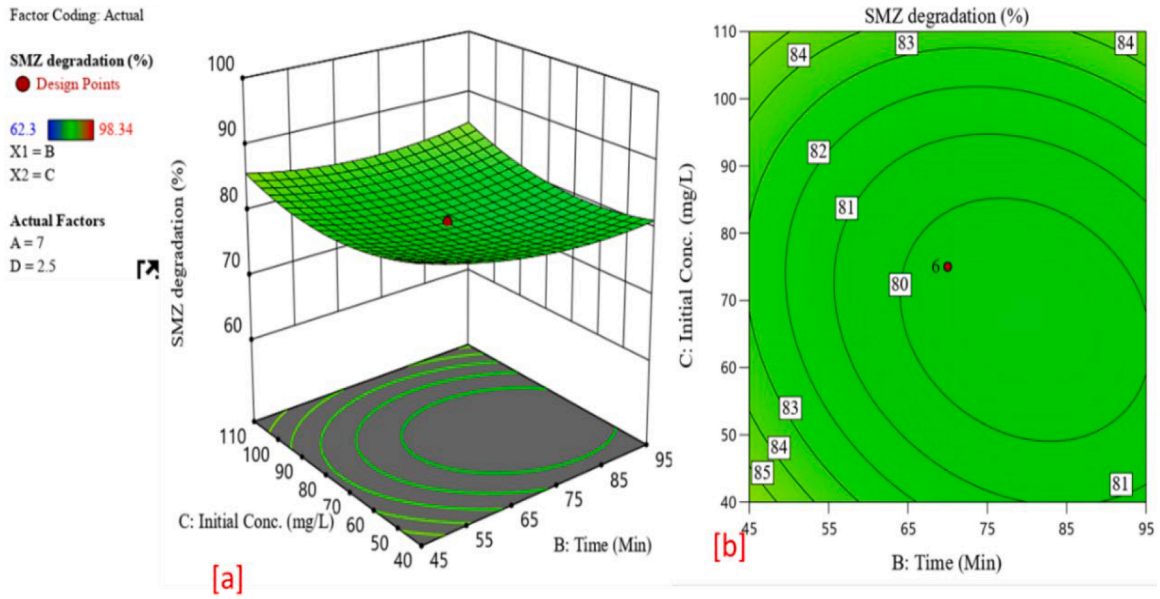


Fig. 12. [a] the 3D response surface, and [b] the 2D contour map showing the interaction of contact time and initial concentration.

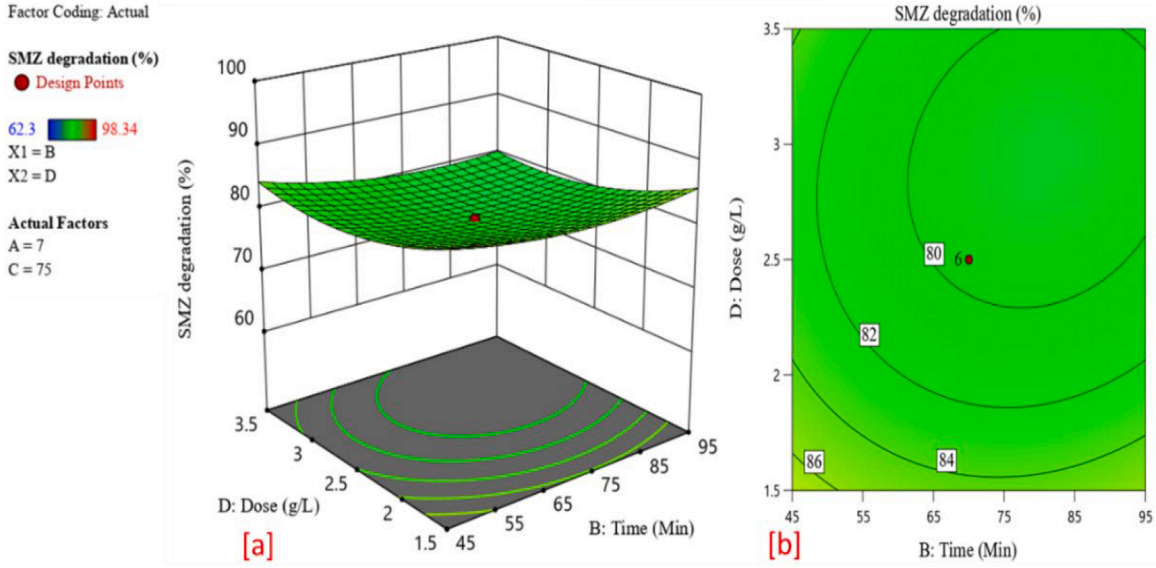


Fig. 13. [a] the 3D response surface, and [b] the 2D contour map showing the interaction of contact time and catalyst dose.

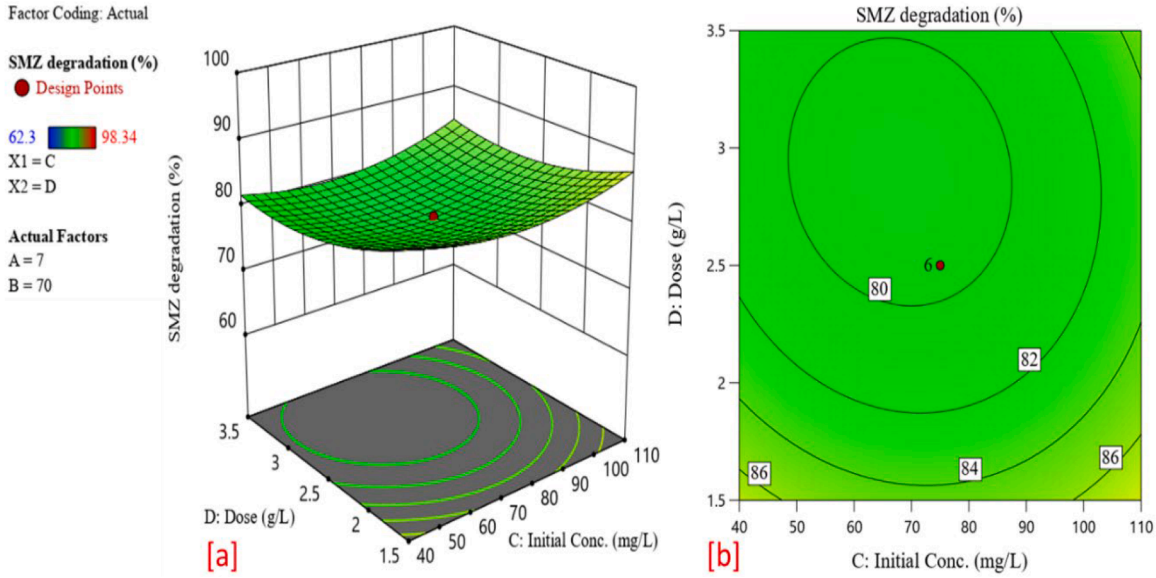


Fig. 14. [a] the 3D response surface and [b] the 2D contour map shows the interaction of initial concentration and catalyst dose.

nanocomposite increases, the particles can scatter and absorb more light, leading to a decrease in the effective light intensity that reaches the photocatalyst. Consequently, this limits the generation of reactive species, such as •OH, which are essential for the degradation of SMZ [94]. Similarly, the degradation efficiency was negatively impacted by increases in the initial concentration of SMZ. As the concentration of SMZ rises, the number of pollutant molecules in the solution increases, leading to a similar light-shielding effect. The higher concentration of SMZ molecules can absorb and scatter light, thereby reducing the amount of light available for activating the photocatalyst. This situation results in a decreased formation of reactive species, which are critical for the effective degradation of the antibiotic [88]. These results emphasize the importance of optimizing both the photocatalyst dosage and the initial pollutant concentration to achieve optimal degradation efficiency. Although it may seem beneficial to increase the amount of photocatalyst to enhance degradation, excessive dosages can lead to diminishing returns due to light shielding. Therefore, a careful balance should be maintained to ensure that sufficient light reaches the photocatalyst while also allowing effective interaction with the pollutant. In conclusion, the results highlight the need for a systematic approach to optimizing photocatalytic processes, particularly in complex wastewater matrices where both the photocatalyst dosage and the concentration of contaminants significantly influence degradation outcomes.

3.5. Photocatalytic degradation mechanism

The degradation mechanisms of SMZ residues were systematically investigated through laboratory experiments using specific chemical scavengers that target distinct reactive species and analyzed via LC-MS. Chemical agents such as PBQ, IPA, EDTA, and $AgNO_3$ were utilized to capture O_2^{-}•, •OH, holes (h^+), and electrons (e^-), respectively. The results indicate that •OH was the primary agent in the degradation of SMZ, achieving a degradation efficiency of 38.5 % as shown in Fig. 15. This relatively low efficiency highlights the complexity of the degradation process and suggests the involvement of other reactive species and

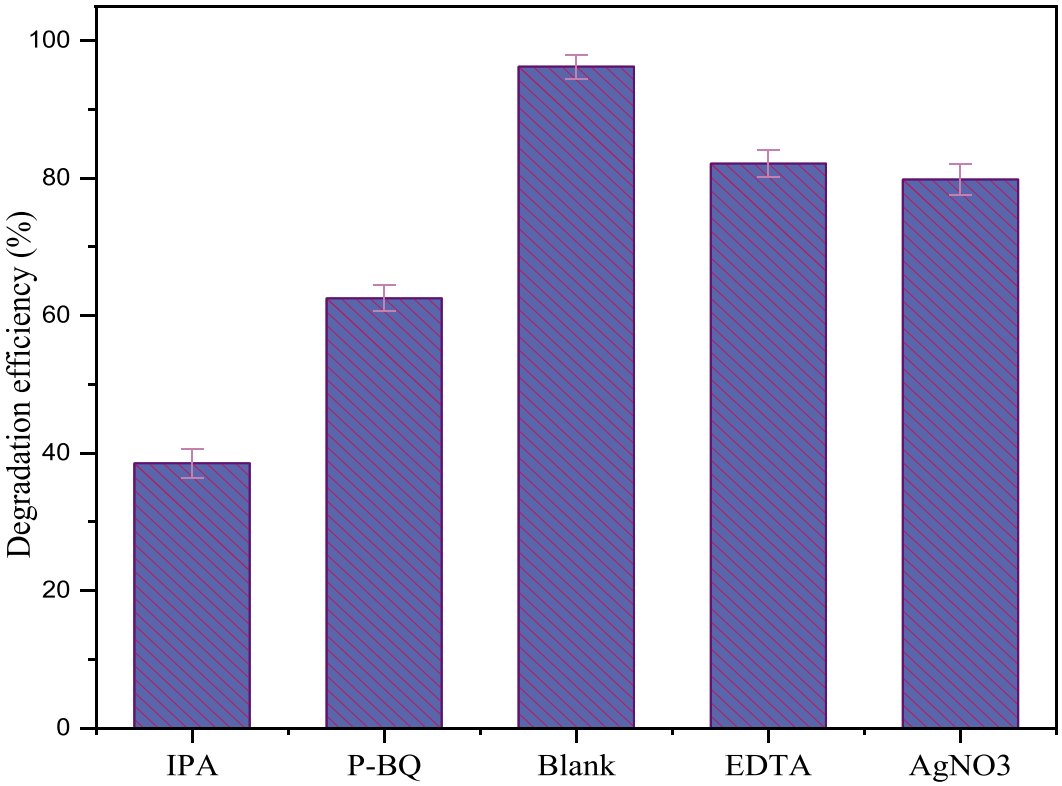


Fig. 15. The influence of different scavengers on the degradation of SMZ by N-doped $TiO_2/BC_{20\ \%}$ nanocomposite.

mechanisms. The experimental findings align with previous studies [96], indicating that while •OH is crucial, other degradation pathways also contribute significantly to the overall process. The degradation mechanism, illustrated in Fig. 16, begins under light exposure, where e^- and h^+ are generated in the CB and VB of the N-doped $TiO_2/BC_{20\ \%}$ nanocomposite, as described in Eq. (2). Surface electrons react with oxygen to produce $\bullet O_2^-$ (Eq. (3)), which then interact with hydrogen ions (H^+) to generate •OH (Eq. (4)). Furthermore, the energy levels of the valence band in the N-doped $TiO_2/BC_{20\ \%}$ nanocomposite facilitate the transfer of h^+ from $TiO_2/BC_{20\ \%}$, promoting the formation of •OH from

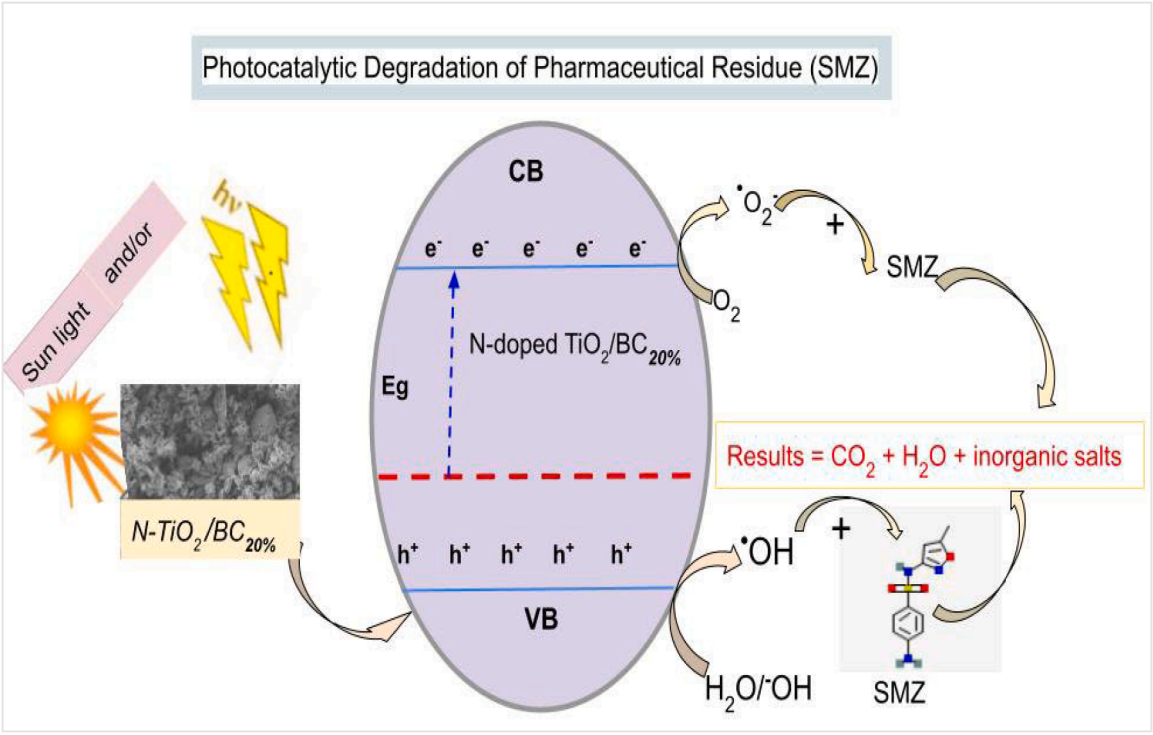


Fig. 16. Photocatalytic degradation mechanism of SMZ by N-doped $TiO_2/BC_{20\ \%}$ nanocomposite.

hydroxyl ions and water molecules (Eq. (5)). These reactive species ultimately assist in breaking down SMZ into less harmful byproducts, such as CO_2 and H_2O, as presented in Eqs. (9) and 10, in accordance with mechanisms identified in similar research [97]. This study emphasizes the importance of the synergistic interactions among reactive species in achieving effective degradation and offers valuable insights for designing advanced photocatalytic systems.

Under UV or visible light, the N-doped TiO_2 in the nanocomposite absorbs photons, which excites electrons from the VB to the CB and creates electron-hole pairs.

$$N - TiO_2BC20\% + hv \rightarrow N - TiO_2BC\ (e^- + h^+) \quad (2a)$$

Electron Transfer to Oxygen:

$$O_2 + e^- \rightarrow O_2^- \quad (3a)$$

Hole Reaction with Water or Hydroxide Ions:

$$h^+ + H_2O \rightarrow OH^{\cdot} + H^+ \quad (4)$$

$$h^+ + OH^- \rightarrow OH^{\cdot} + H^+ \quad (5)$$

Formation of Reactive Species:

$$O^- + H^+ \rightarrow HO_2 \quad (6)$$

$$2HO_2^{\cdot} \rightarrow H_2O_2 + O_2 \quad (7)$$

$$H_2O_2 + e^- \rightarrow OH^{\cdot} + OH^- \quad (8)$$

Degradation of Pollutants

$$R + OH^{\cdot} \rightarrow Degraded\ products\ (H2O + CO2 + Inorganic\ salts) \quad (9)$$

$$R + O_2^- \rightarrow Degradation\ Products(H2O + CO2 + Inorganic\ salts) \quad (10)$$

These equations collectively describe the degradation mechanisms when using an N-doped $TiO_2/BC_{20\ \%}$ nanocomposite as a photocatalyst. The process involves light absorption, the generation of reactive species, and the subsequent breakdown of pollutants into less harmful substances.

On the other hand, the photocatalytic degradation of pharmaceutical wastewater using an N-doped $TiO_2/BC_{20\ \%}$ nanocomposite is illustrated in Fig. 17. Significant interference from common anions was observed, with Sodium Dodecyl Sulfate (SDS) exhibiting the highest inhibition at 52.4 %. This was followed by chlorides (Cl^-) at 34.8 %, sulfates (SO_4^{2-}) at 27.4 %, and nitrates (NO_3^-) at 11.9 %. These interferences can be attributed to competitive adsorption and radical scavenging effects, which hinder the degradation efficiency of organic pollutants. SDS demonstrated the strongest inhibitory effect, likely due to its surfactant properties, which compete for active sites on the N-doped TiO_2/BC surface and form micelles that reduce the availability of •OH [98]. Chlorides also significantly reduced degradation efficiency, possibly by reacting with the photogenerated h^+ ions to form less reactive chlorine radicals (•Cl), as reported in previous studies [99]. Sulfates exhibited moderate interference, likely due to their ability to scavenge hydroxyl radicals, forming sulfate radicals ($SO_4^{\bullet-}$) that possess lower oxidative potential [100]. Nitrates had the least impact, possibly because they primarily compete for conduction band electrons rather than directly quenching ROS [101,102]. These findings align with earlier studies on anion interference in photocatalytic systems, highlighting the need for pretreatment or optimized nanocomposite design to mitigate competitive effects in complex wastewater matrices.

3.6. Photocatalysis of pharmaceutical wastewater

The N-doped $TiO_2/BC_{20\ \%}$ nanocomposite, refined using RSM, shows significant potential for real-world wastewater treatment applications. With optimal operational parameters identified as 95 min of agitation time, pH 5, a SMZ concentration of 110 mg/L, and a nanocomposite dosage of 1.5 g/L, the composite achieved impressive removal efficiencies of 98.3 % for synthetic wastewater and 86.6 % for real pharmaceutical industry wastewater at a laboratory scale. These results underscore the practical applicability of nanocomposites in treating complex organic pollutants typically found in water. Real pharmaceutical wastewater often contains diverse contaminants and complex matrices, which can reduce treatment efficiency compared to synthetic samples [103]. Despite these challenges, the high removal efficiency demonstrated by the nanocomposite in real wastewater highlights its robustness and adaptability for environmental remediation [104]. The enhanced light-harvesting ability and reduced electron recombination of the nanocomposite contribute to its superior photocatalytic

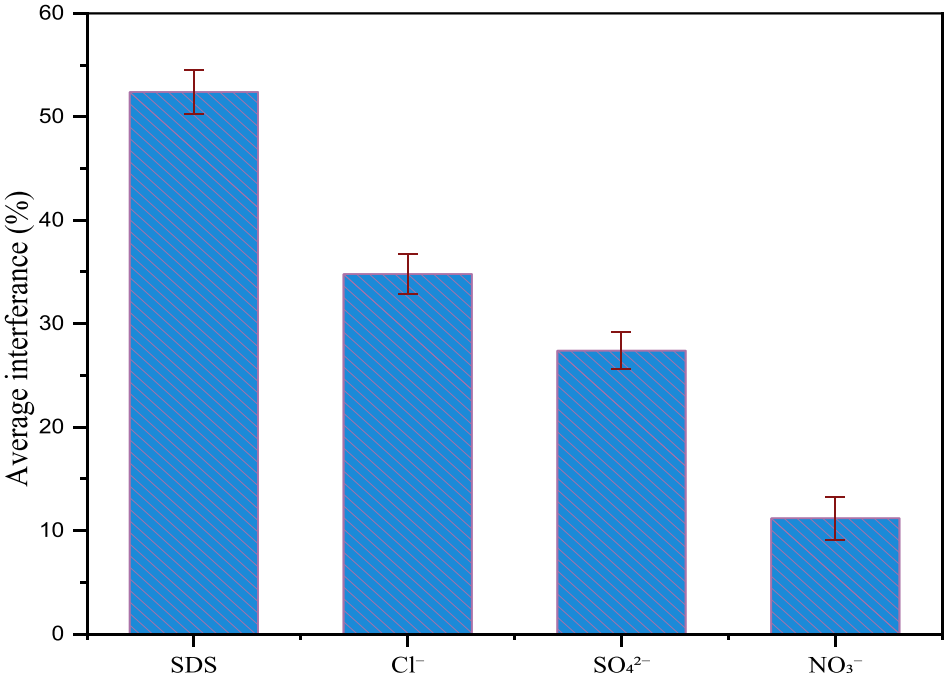


Fig. 17. Average interference of pharmaceutical wastewater constituents on photocatalytic degradation.

performance. These properties enable the effective degradation of pharmaceutical pollutants under natural sunlight, making the process both energy-efficient and cost-effective [105,106]. When applied under sunlight, the synthesized nanocomposite achieved a removal efficiency of 97.3 %, matching the performance of UV light. Additionally, the presence of interfering ions complicates the treatment of real pharmaceutical wastewater, as evidenced by the differences in results between synthetic and real wastewater. Although the method is effective at the laboratory scale, scaling it up for the treatment of pharmaceutical residues presents common challenges associated with advanced oxidation processes (AOP): uniform mixing in larger volumes [107], maintaining reaction efficiency in continuous flow, and energy demands [108]. Similarly, emerging technologies, including hybrid systems, may address these limitations, though pilot-scale validation is essential for practical implementation [109]. Furthermore, the use of N-doped $TiO_2/BC_{20\ \%}$ nanocomposites offers a sustainable and economically attractive approach to addressing pharmaceutical residues and other micro-pollutant organic pollutants in real wastewater environments. By integrating this technology into water and wastewater treatment systems, it is possible to achieve efficient pollutant removal, thereby tackling the increasing environmental challenges posed by pharmaceutical residues in water bodies.

3.7. Reusability and stability test

The effectiveness of N-doped $TiO_2/BC_{20\ \%}$ for degrading SMZ was assessed over six successive cycles, showing promising efficiency levels, as illustrated in Fig. 18. Initially, the catalyst achieved a degradation rate of 98.6 %. However, this rate slightly decreased with continued use, dropping to 89.2 % by the sixth cycle. This pattern indicates that while the material retains significant catalytic effectiveness across multiple applications, there are minor losses in efficiency, likely due to structural changes or partial deactivation of active sites over time [91]. These results highlight the robustness of N-doped $TiO_2/BC_{20\ \%}$, confirming its suitability for repeated use in wastewater treatment. The observed decline in performance can be attributed to several factors, such as the accumulation of by-products on the catalyst's surface and the potential leaching of active components. Nevertheless, even after six cycles, the degradation efficiency remains relatively high, demonstrating the material's durability and sustainability. To enhance long-term effectiveness, further optimization strategies, including occasional regeneration or adjustments to the catalyst, may be beneficial. Overall, the study underscores the potential of N-doped $TiO_2/BC_{20\ \%}$ as an effective and reusable photocatalyst for environmental cleanup initiatives.

4. Conclusion

This study effectively optimized the photocatalytic degradation of SMZ in real pharmaceutical wastewater using an N-doped $TiO_2/BC_{20\ \%}$ nanocomposite. Under the optimized conditions (an agitation time of 95 min, a pH of 5, a nanocomposite dosage of 1.5 g/L, and an SMZ concentration of 110 mg/L), the removal efficiency reached 98.3 %. The optimization process, guided by RSM, confirmed the reliability of the quadratic model, which demonstrated an R^2 value of 0.999 and a non-significant lack of fit ($p = 0.3014$), ensuring a robust experimental design. Mechanistic studies identified •OH (61.5 %) and O_2^{-}• (37.5 %) as the primary reactive species responsible for the degradation of SMZ. Furthermore, the nanocomposite displayed remarkable durability, maintaining efficiency across over 6 cycles with less than a 5 % loss. It also performed admirably in real wastewater, achieving an 86.6 % degradation of SMZ, thereby confirming its practical applicability. These findings carry substantial implications for the treatment of pharmaceutical wastewater, as conventional methods often fall short of eliminating SMZ. Beyond controlled laboratory conditions, the results highlight the significance of sustainable wastewater treatment. With its high efficiency, activation under visible light (97.3 %) and reusability, the nanocomposite emerges as a promising alternative for water purification. However, the successful large-scale application of this technology will require addressing several key challenges, including the scalability of synthesis, long-term stability, and integration into continuous-flow systems. Future research should aim to refine the catalyst's composition to enhance degradation efficiency under varying

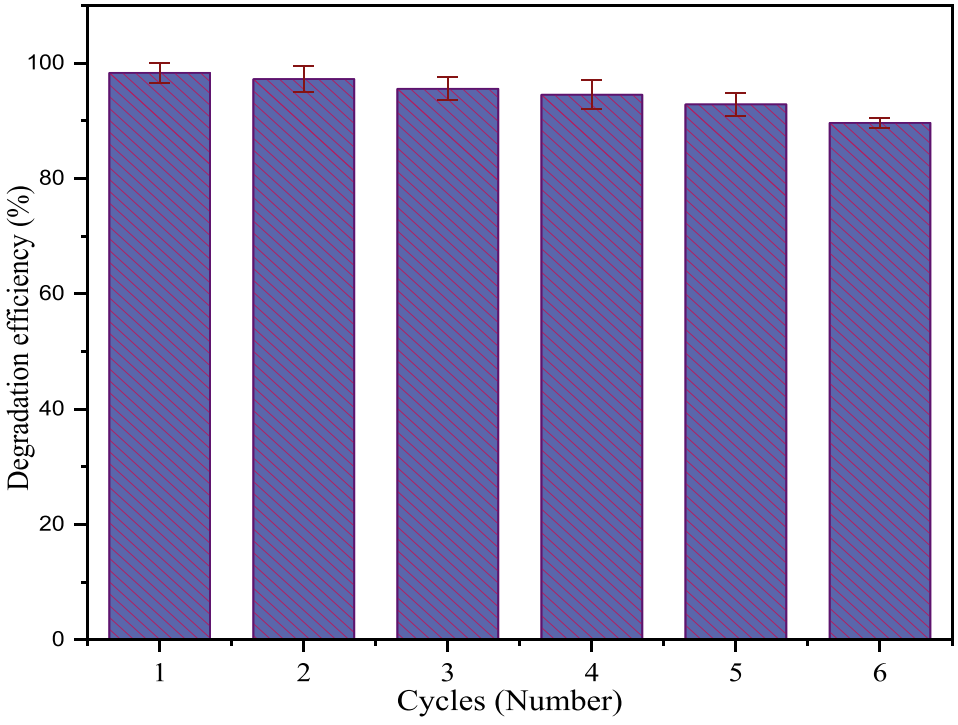


Fig. 18. Stability test of N-doped $TiO_2/BC_{20\ \%}$ nanocomposite for SMZ antibiotic degradation under agitation time of 95 min, a pH of 5, a nanocomposite dosage of 1.5 g/L, and an SMZ concentration of 110 mg/L.

environmental conditions and minimize the potential for secondary pollutants. Additionally, advancements in photocatalytic reactor design and engineering will be crucial for improving operational feasibility. Incorporating hybrid treatment approaches, such as combining photocatalysis with membrane filtration, could further enhance overall treatment performance. This study contributes to the advancement of effective, scalable, and environmentally friendly wastewater treatment technologies, offering a viable solution for mitigating pharmaceutical pollution and enhancing water quality management.

Funding information

This research did not receive any specific grant from funding agencies in the public, commercial, or not-for-profit sectors.

Availability of data

All data are fully available without restriction from the corresponding author.

Ethical statement

This manuscript does not require an ethical statement, as the research conducted did not involve human subjects, animals, or sensitive data that necessitate ethical review.

CRediT authorship contribution statement

Hailu Ashebir: Writing – review & editing, Writing – original draft, Software, Methodology, Investigation, Formal analysis, Conceptualization. **Saeideh Babaee:** Writing – review & editing, Writing – original draft, Methodology, Conceptualization. **Palesa Diale:** Writing – review & editing, Writing – original draft, Methodology, Conceptualization. **Abebe Worku:** Writing – review & editing, Writing – original draft, Formal analysis, Data curation, Conceptualization. **T.A.M. Msagati:** Writing – review & editing, Writing – original draft, Methodology, Conceptualization. **Jemal Fito Nure:** Writing – review & editing, Writing – original draft, Visualization, Validation, Supervision, Software, Methodology, Formal analysis, Data curation, Conceptualization.

Declaration of competing interest

The authors declare that they have no known competing financial interests or personal relationships that could have appeared to influence the work reported in this paper.

The authors declare the following financial interests/personal relationships which may be considered as potential competing interests:

No one is the potential competing interest!!!

Data availability

Data will be made available on request.

References

[1] S.A.R. Ahmadi, M.R. Kalaee, O. Moradi, F. Nosratinia, M. Abdouss, Core–shell activated carbon-ZIF-8 nanomaterials for the removal of tetracycline from polluted aqueous solution, Adv. Compos. Hybrid. Mater. 4 (2021) 1384–1397.

[2] J. Rauseo, A. Barra Caracciolo, F. Spataro, A. Visca, N. Ademollo, T. Pescatore, et al., Effects of sulfamethoxazole on growth and antibiotic resistance of a natural microbial community, Water. (Basel) 13 (2021) 1262.

[3] A. Singh, S.G. Pratap, A. Raj, Occurrence and dissemination of antibiotics and antibiotic resistance in aquatic environment and its ecological implications: a review, Environ. Sci. Pollut. Res. 31 (2024) 47505–47529.

[4] N. Puhlmann, R. Vidaurre, K. Kümmerer, Designing greener active pharmaceutical ingredients: insights from pharmaceutical industry into drug discovery and development, Eur. J. Pharm. Sci. 192 (2024) 106614.

[5] J.I. Nieto-Juárez, R.A. Torres-Palma, A.M. Botero-Coy, F. Hernández, Pharmaceuticals and environmental risk assessment in municipal wastewater treatment plants and rivers from Peru, Environ. Int. 155 (2021) 106674.

[6] M.I. Sahadulla, S.A. Uduman, Comprehensive Textbook of Infectious Diseases, Jaypee Brothers Medical Publishers, 2019.

[7] S. Li, N. Hofstra, M.G.M. van de Schans, J. Yang, Y. Li, Q. Zhang, et al., Riverine antibiotics from animal production and wastewater, Environ. Sci. Technol. Lett. 10 (2023) 1059–1067.

[8] P.K. Singh, N. Ranjan, Ecological impact of pharmaceutical pollutants and options of river health improvements - A risk analysis-based approach, Sci. Total. Environ. 928 (2024) 172358, https://doi.org/10.1016/j.scitotenv.2024.172358.

[9] M. Abdu, S. Tibebu, S. Babaee, A. Worku, T.A.M. Msagati, J.F. Nure, Optimization of photocatalytic degradation of eriochrome Black T from aqueous solution using TiO2-biochar composite, Results. Eng. 25 (2025) 104036, https://doi.org/10.1016/j.rineng.2025.104036.

[10] S.A.R. Ahmadi, M.R. Kalaee, O. Moradi, F. Nosratinia, M. Abdouss, Synthesis of novel zeolitic imidazolate framework (ZIF-67)–zinc oxide (ZnO) nanocomposite (ZnO@ ZIF-67) and potential adsorption of pharmaceutical (tetracycline (TCC)) from water, J. Mol. Struct. 1251 (2022) 132013.

[11] S.M. Samianifard, M. Kalaee, O. Moradi, N.M. Mahmoodi, D. Zaarei, Synthesis of novel starch/zeolitic imidazolate framework (ZIF-67)/graphene oxide biocomposite and photocatalytic dye degradation ability, Opt. Mater. (Amst) 151 (2024) 115268, https://doi.org/10.1016/j.optmat.2024.115268.

[12] S. Mohammad Samianifard, M. Kalaee, O. Moradi, N.M. Mahmoodi, D. Zaarei, Novel biocomposite (Starch/metal–organic framework /Graphene oxide): synthesis, characterization and visible light assisted dye degradation, J. Photochem. Photobiol. a Chem. 450 (2024) 115417, https://doi.org/10.1016/j.jphotochem.2023.115417.

[13] O. Moradi, H. Alizadeh, S. Sedaghat, Removal of pharmaceuticals (diclofenac and amoxicillin) by maltodextrin/reduced graphene and maltodextrin/reduced graphene/copper oxide nanocomposites, Chemosphere 299 (2022) 134435, https://doi.org/10.1016/j.chemosphere.2022.134435.

[14] N.A. Khan, S.U. Khan, S. Ahmed, I.H. Farooqi, M. Yousefi, A.A. Mohammadi, et al., Recent trends in disposal and treatment technologies of emerging-pollutants-A critical review, TrAC Trends Anal. Chem. 122 (2020) 115744.

[15] S. de Boer, J. González-Rodríguez, J.J. Conde, M.T. Moreira, Benchmarking tertiary water treatments for the removal of micropollutants and pathogens based on operational and sustainability criteria, J. Water. Process. Eng. 46 (2022) 102587.

[16] J. Khodayari, K. Zare, O. Moradi, M. Kalaee, N. Mohammad Mahmoodi, Synthesis of eco-friendly carboxymethyl cellulose /metal–organic framework biocomposite and its photocatalytic activity, J. Photochem. Photobiol. a Chem. 446 (2024) 115097, https://doi.org/10.1016/j.jphotochem.2023.115097.

[17] B. Farahani, M. Giahi, M.H. Ghorbani, R. Fazaeli, O. Moradi, Synthesis of CuS/NiS heterostructural photocatalyst and its performance in the degradation of metronidazole and diclofenac drugs: optimization of operating conditions, J. Nanostructure Chem. 13 (2023) 303–320.

[18] M. SefidSiahbandi, O. Moradi, B. Akbari –adergani, P.A. Azar, M.S Tehrani, Fabrication and implementation of bimetallic Fe/Zn nanoparticles (mole ratio 1: 1) loading on hydroxyethylcellulose – Graphene oxide for removal of tetracycline antibiotic from aqueous solution, Chemosphere 312 (2023) 137184, https://doi.org/10.1016/j.chemosphere.2022.137184.

[19] F. Farzi, K. Zare, O. Moradi, K. Larijani, Adsorptive removal of oxytetracycline antibiotic from graphene oxide nanocomposite modified with magnesium oxide and methyl methacrylate, Iran J. Chem. Chem. Eng. (IJCCE) Res. Artic Vol. (2024) 43.

[20] M. SefidSiahbandi, O. Moradi, B. Akbari–adergani, P. Aberoomand Azar, M. Sabar Tehrani, The effect of Fe–Zn mole ratio (2:1) bimetallic nanoparticles supported by hydroxyethyl cellulose/graphene oxide for high-efficiency removal of doxycycline, Environ. Res. 218 (2023) 114925, https://doi.org/10.1016/j.envres.2022.114925.

[21] S. Satyam, S. Patra, Innovations and Challenges in Adsorption-Based Wastewater Wemediation: a Comprehensive Review, Heliyon, 2024.

[22] Y. Dai, N. Zhang, C. Xing, Q. Cui, Q. Sun, The adsorption, regeneration and engineering applications of biochar for removal organic pollutants: a review, Chemosphere 223 (2019) 12–27, https://doi.org/10.1016/j.chemosphere.2019.01.161.

[23] W. Qin, Y. Dong, H. Jiang, W.H. Loh, J. Imbrogno, T.M. Swenson, et al., A new approach of simultaneous adsorption and regeneration of activated carbon to address the bottlenecks of pharmaceutical wastewater treatment, Water. Res. 252 (2024) 121180, https://doi.org/10.1016/j.watres.2024.121180.

[24] Z. Bai, Q. Yang, J. Wang, Catalytic ozonation of sulfamethazine antibiotics using Fe3O4/multiwalled carbon nanotubes, Environ. Prog. Sustain. Energy 37 (2018) 678–685.

[25] X. Liu, F. Huang, Y. Yu, Y. Jiang, K. Zhao, Y. He, et al., Determination and toxicity evaluation of the generated byproducts from sulfamethazine degradation during catalytic oxidation process, Chemosphere 226 (2019) 103–109.

[26] I.A. Katsoyiannis, S. Canonica, U. von Gunten, Efficiency and energy requirements for the transformation of organic micropollutants by ozone, O3/H2O2 and UV/H2O2, Water. Res. 45 (2011) 3811–3822.

[27] T. Manasfi, Chapter four - ozonation in drinking water treatment: an overview of general and practical aspects, mechanisms, kinetics, and byproduct formation, in: T. Manasfi, J-L Boudenne (Eds.), Anal. Form. Disinfect. Byprod. Drink. Water, editorsAnal. Form. Disinfect. Byprod. Drink. Water, 92, Elsevier, 2021, pp. 85–116, https://doi.org/10.1016/bs.coac.2021.02.003.

[28] N. Madkhali, C. Prasad, K. Malkappa, H.Y. Choi, V. Govinda, I. Bahadur, et al., Recent update on photocatalytic degradation of pollutants in waste water using TiO2-based heterostructured materials, Results. Eng. 17 (2023) 100920, https://doi.org/10.1016/j.rineng.2023.100920.

[29] W. Yuan, X. Chen, Z. Yu, Y. Wan, J. Lin, W. Ye, Critical review of membrane fouling in reverse osmosis treatment: characterizations, models, mechanisms, and controls, Sep. Purif. Technol. 363 (2025) 132119, https://doi.org/10.1016/j.seppur.2025.132119.

[30] H.J. Tanudjaja, A. Anantharaman, A.Q.Q. Ng, Y. Ma, M.B. Tanis-Kanbur, A. L. Zydney, et al., A review of membrane fouling by proteins in ultrafiltration and microfiltration, J. Water. Process. Eng. 50 (2022) 103294, https://doi.org/10.1016/j.jwpe.2022.103294.

[31] D. Kanakaraju, B.D. Glass, M. Oelgemöller, Advanced oxidation process-mediated removal of pharmaceuticals from water: a review, J. Environ. Manage 219 (2018) 189–207, https://doi.org/10.1016/j.jenvman.2018.04.103.

[32] J. Iqbal, N.S. Shah, J.A. Khan, M. Naushad, G. Boczkaj, F. Jamil, et al., Pharmaceuticals wastewater treatment via different advanced oxidation processes: reaction mechanism, operational factors, toxicities, and cost evaluation–A review, Sep. Purif. Technol. (2024) 127458.

[33] Gaggero E. Integrated sustainable approach aimed to develop combined systems for achieving the environmental recovery of water bodies 2024.

[34] A. de Wilt, M.J. Arlos, M.R. Servos, H.H.M. Rijnaarts, A.A.M. Langenhoff, W. J. Parker, Improved biodegradation of pharmaceuticals after mild photocatalytic pretreatment, Water. Environ. J. 34 (2020) 704–714.

[35] R. Kumar, E. Awino, D.W. Njeri, A. Basu, S. Chattaraj, J. Nayak, et al., Advancing pharmaceutical wastewater treatment: a comprehensive review on application of catalytic membrane reactor-based hybrid approaches, J. Water. Process. Eng. 58 (2024) 104838.

[36] F.H. Kamil, S.K.A. Barno, F. Shems, A. Jihad, A.S. Abbas, Photocatalytic degradation of sulfamethoxazole from a synthetic pharmaceutical wastewater using titanium dioxide (TiO2) powder as a suspended heterogeneous catalyst, Iraqi J. Ind. Res. 10 (2023) 26–33.

[37] C.B. Ong, L.Y. Ng, A.W. Mohammad, A review of ZnO nanoparticles as solar photocatalysts: synthesis, mechanisms and applications, Renew. Sustain. Energy Rev. 81 (2018) 536–551.

[38] R. Djellabi, L. Noureen, V.D. Dao, D. Meroni, E. Falletta, D.D. Dionysiou, et al., Recent advances and challenges of emerging solar-driven steam and the contribution of photocatalytic effect, Chem. Eng. J. 431 (2022) 134024, https://doi.org/10.1016/j.cej.2021.134024.

[39] S. Marathe, Ł. Sadowski, Developments in biochar incorporated geopolymers and alkali activated materials: a systematic literature review, J. Clean. Prod. (2024) 143136.

[40] M. Hosseini, M. Ghanbari, E.A. Dawi, M.H. Shuhata Alubiady, A.M. Al-Ani, A. F. Alkaim, et al., CaSnO3/g-C3N4 S-scheme heterojunction photocatalyst for the elimination of erythrosine and eriochrome black T from water under visible light, Results. Eng. 21 (2024) 101903, https://doi.org/10.1016/j.rineng.2024.101903.

[41] S. Ariaeenejad, K. Kavousi, M. Zeinalabedini, D. Afshar Jahanshahi, S.R Beh-Afarin, Enhanced bioremediation of saline azo dye effluents using PersiLac3: a thermo-halotolerant laccase from a tannery metagenome, Results. Eng. 24 (2024) 103172, https://doi.org/10.1016/j.rineng.2024.103172.

[42] P. Cervantes-Avilés, J. Ida, T. Toda, G. Cuevas-Rodríguez, Effects and fate of TiO2 nanoparticles in the anaerobic treatment of wastewater and waste sludge, J. Environ. Manage 222 (2018) 227–233.

[43] M. Delarmelina, M.W. Dlamini, S. Pattisson, P.R. Davies, G.J. Hutchings, C.R. A. Catlow, The effect of dissolved chlorides on the photocatalytic degradation properties of titania in wastewater treatment, Phys. Chem. Chem. Phys. 25 (2023) 4161–4176.

[44] S. Alomairy, L. Gnanasekaran, S. Rajendran, W.F. Alsanie, Biochar supported nano core-shell (TiO2/CoFe2O4) for wastewater treatment, Environ. Res. 238 (2023) 117169.

[45] S. Chandra, P. Jagdale, I. Medha, A.K. Tiwari, M. Bartoli, NinoA De, et al., Biochar-supported TiO2-based nanocomposites for the photocatalytic degradation of sulfamethoxazole in water—A review, Toxics. 9 (2021) 313.

[46] O.O. Olabinjo, Response surface techniques as an inevitable tool in optimization process, Response Surf. methods-Theory, Appl. Optim. Tech. (2024). IntechOpen.

[47] M.Z. Akbari, Y. Xu, C. Liang, Z. Lu, S. Shen, L. Peng, Synthesis of ZnO@ VC for enhancement of synergic photocatalytic degradation of SMX: toxicity assessment, kinetics and transformation pathway determination, Chem. Eng. Process Intensif. 193 (2023) 109544.

[48] S.P. Fauziyen, W.H. Saputera, D. Sasongko, Advancement and prospects in photocatalytic degradation of sulfamethoxazole (SMX) pharmaceutical waste, South Afr. J. Chem. Eng. 48 (2024) 375–394.

[49] V. Katheresan, J. Kansedo, S.Y. Lau, Efficiency of various recent wastewater dye removal methods: a review, J. Environ. Chem. Eng. 6 (2018) 4676–4697, https://doi.org/10.1016/j.jece.2018.06.060.

[50] H. Ashebir, J.F. Nure, A. Worku, T.A.M. Msagati, Prosopis Juliflora biochar for adsorption of sulfamethoxazole and ciprofloxacin from pharmaceutical wastewater, Desalin Water Treat (2024) 100691.

[51] J. Assunção, F.X. Malcata, Enclosed "non-conventional" photobioreactors for microalga production: a review, Algal. Res. 52 (2020) 102107.

[52] A. Queral-Beltran, M. Marín-García, S. Lacorte, R. Tauler, UV-vis absorption spectrophotometry and LC-DAD-MS-ESI(+)-ESI(−) coupled to chemometrics analysis of the monitoring of sulfamethoxazole degradation by chlorination, photodegradation, and chlorination/photodegradation, Anal. Chim. Acta 1276 (2023) 341563, https://doi.org/10.1016/j.aca.2023.341563.

[53] L.H. Shindume, Z. Zhao, N. Wang, H. Liu, A. Umar, J. Zhang, et al., Enhanced photocatalytic activity of B, N-codoped TiO2 by a new molten nitrate process, J. Nanosci. Nanotechnol. 19 (2019) 839–849.

[54] D.E. Athanasaki, S.D. Georgiou, S. Stylianou, New approaches on composite designs for Response Surface Methodology, PLoS. One 19 (2024) e0301049.

[55] J. Dang, W. Pei, F. Hu, Z. Yu, S. Zhao, J. Hu, et al., Photocatalytic degradation and Toxicity analysis of sulfamethoxazole using TiO2/BC, Toxics. 11 (2023) 818.

[56] K. Masuda, T. Ichitsuka, N. Koumura, K. Sato, S. Kobayashi, Flow fine synthesis with heterogeneous catalysts, Tetrahedron. 74 (2018) 1705–1730.

[57] M. Borelli, A. Bergomi, V. Comite, V. Guglielmi, C.A. Lombardi, S. Gilardoni, et al., Development of a new analytical method for the characterization and quantification of the organic and inorganic carbonaceous fractions in snow samples using TOC and TOT analysis, Atmosphere (Basel) 14 (2023) 371.

[58] J. Li, X. Deng, R. Guo, B. Li, Q. Cheng, X. Cheng, Visible light driven photocatalytic decomposition of penicillin G by Ti3+ self-doped TiO2 nano-catalyst through response surface methodology, J. Taiwan. Inst. Chem. Eng. 87 (2018) 174–181, https://doi.org/10.1016/j.jtice.2018.03.033.

[59] A.I. Mundo, J.R. Tipton, T.J. Muldoon, Generalized additive models to analyze nonlinear trends in biomedical longitudinal data using R: beyond repeated measures ANOVA and linear mixed models, Stat. Med. 41 (2022) 4266–4283.

[60] N. Khoshnamvand, F. Kord Mostafapour, A. Mohammadi, M. Faraji, Response surface methodology (RSM) modeling to improve removal of ciprofloxacin from aqueous solutions in photocatalytic process using copper oxide nanoparticles (CuO/UV), AMB Express. 8 (2018) 1–9.

[61] I. Salahshoori, M.N. Jorabchi, A. Baghban, H.A. Khonakdar, Integrative analysis of multi machine learning models for tetracycline photocatalytic degradation with MOFs in wastewater treatment, Chemosphere 350 (2024) 141010.

[62] S. Feng, J. Liu, B. Gao, L. Bo, L. Cao, The filtration and degradation mechanism of toluene via microwave thermo-catalysis ceramic membrane, J. Environ. Chem. Eng. 9 (2021) 105105.

[63] D.R. Eddy, M.D. Permana, L.K. Sakti, G.A.N. Sheha, HidayatS Solihudin, et al., Heterophase polymorph of TiO2 (Anatase, Rutile, Brookite, TiO2 (B)) for efficient photocatalyst: fabrication and activity, Nanomaterials 13 (2023) 704.

[64] S.J. Armaković, M.M. Savanović, S. Armaković, Titanium dioxide as the most used photocatalyst for water purification: an overview, Catalysts. 13 (2022) 26.

[65] X. Chen, S.S. Mao, Titanium dioxide nanomaterials: synthesis, properties, modifications, and applications, Chem. Rev. 107 (2007) 2891–2959.

[66] X. Kang, S. Liu, Z. Dai, Y. He, X. Song, Z. Tan, Titanium dioxide: from engineering to applications, Catalysts. 9 (2019) 191.

[67] T. Parangi, M.K. Mishra, Titania nanoparticles as modified photocatalysts: a review on design and development, Comments Inorg. Chem. 39 (2019) 90–126.

[68] T. Fazal, A. Razzaq, F. Javed, A. Hafeez, N. Rashid, U.S. Amjad, et al., Integrating adsorption and photocatalysis: a cost effective strategy for textile wastewater treatment using hybrid biochar-TiO2 composite, J. Hazard. Mater. 390 (2020) 121623.

[69] Hosseini-monfared H., Mohammadi Y., Montazeri R., Gasemzadeh S., Varma R.S. Effect of biochar on the photocatalytic activity of nitrogen-doped titanium dioxide nanocomposite in the removal of aqueous organic pollutants under visible light illumination 2021;6:79–93. https://doi.org/10.22036/ncr.2021.01.008.

[70] A. Kumar, A. Rana, G. Sharma, M. Naushad, P. Dhiman, A. Kumari, et al., Recent advances in nano-fenton catalytic degradation of emerging pharmaceutical contaminants, J. Mol. Liq. 290 (2019) 111177, https://doi.org/10.1016/j.molliq.2019.111177.

[71] C. Zhang, S. Bengio, M. Hardt, B. Recht, O. Vinyals, Understanding deep learning (still) requires rethinking generalization, Commun ACM 64 (2021) 107–115.

[72] H. Kumari, Suman Sonia, R. Ranga, S. Chahal, S. Devi, et al., A review on photocatalysis used for wastewater treatment: dye degradation, Water, Air, Soil Pollut. 234 (2023) 349.

[73] B.L. Phoon, C.C. Ong, M.S. Mohamed Saheed, P.L. Show, J.S. Chang, T.C. Ling, et al., Conventional and emerging technologies for removal of antibiotics from wastewater, J. Hazard. Mater. 400 (2020) 122961, https://doi.org/10.1016/J.JHAZMAT.2020.122961.

[74] C. Peng, W. Fan, Q. Li, W. Han, X. Chen, G. Zhang, et al., Boosting photocatalytic activity through tuning electron spin states and external magnetic fields, J. Mater. Sci. Technol. 115 (2022) 208–220.

[75] D. Chen, Y. Cheng, N. Zhou, P. Chen, Y. Wang, K. Li, et al., Photocatalytic degradation of organic pollutants using TiO2-based photocatalysts: a review, J. Clean. Prod. 268 (2020) 121725.

[76] H. Wang, W. He, H. Wang, F. Dong, In situ FT-IR investigation on the reaction mechanism of visible light photocatalytic NO oxidation with defective g-C3N4, Sci. Bull. 63 (2018) 117–125.

[77] F. Zhang, X. Wang, H. Liu, C. Liu, Y. Wan, Y. Long, et al., Recent advances and applications of semiconductor photocatalytic technology, Appl. Sci. 9 (2019) 2489.

[78] A. Kumar, Y. Singla, M. Sharma, A. Bhardwaj, V. Krishnan, Two dimensional S-scheme Bi2WO6–TiO2–Ti3C2 nanocomposites for efficient degradation of organic pollutants under natural sunlight, Chemosphere 308 (2022) 136212.

[79] R.K. Sharma, S. Yadav, S. Dutta, H.B. Kale, I.R. Warkad, R. Zboril, et al., Silver nanomaterials: synthesis and (electro/photo) catalytic applications, Chem. Soc. Rev. 50 (2021) 11293–11380.

[80] N. Ali, A. Said, F. Ali, F. Raziq, Z. Ali, M. Bilal, et al., Photocatalytic degradation of congo red dye from aqueous environment using cobalt ferrite nanostructures: development, characterization, and photocatalytic performance, Water, Air, Soil Pollut 231 (2020) 1–16.

[81] Y. Nam, J.H. Lim, K.C. Ko, J.Y. Lee, Photocatalytic activity of TiO 2 nanoparticles: a theoretical aspect, J Mater Chem A 7 (2019) 13833–13859.
[82] M.G. Shirkoohi, R.D. Tyagi, P.A. Vanrolleghem, P. Drogui, Modelling and optimization of psychoactive pharmaceutical caffeine removal by electrochemical oxidation process: a comparative study between response surface methodology (RSM) and adaptive neuro fuzzy inference system (ANFIS), Sep. Purif. Technol. 290 (2022) 120902.
[83] K.E. Tollefsen, L. Nizzetto, D.B. Huggett, Presence, fate and effects of the intense sweetener sucralose in the aquatic environment, Sci. Total. Environ. 438 (2012) 510–516, https://doi.org/10.1016/j.scitotenv.2012.08.060.
[84] J. Musial, D.T. Mlynarczyk, B.J. Stanisz, Photocatalytic degradation of sulfamethoxazole using TiO2-based materials – Perspectives for the development of a sustainable water treatment technology, Sci. Total. Environ. 856 (2023) 159122, https://doi.org/10.1016/J.SCITOTENV.2022.159122.
[85] M. Binazadeh, J. Rasouli, S. Sabbaghi, S.M. Mousavi, S.A. Hashemi, C.W. Lai, An overview of photocatalytic membrane degradation development, Materials. (Basel) 16 (2023) 3526.
[86] S.A. Abdulrahman, Z.Y. Shnain, S.S. Ibrahim, H.S. Majdi, Photocatalytic degradation of ciprofloxacin by UV light using n-doped TiO2 in suspension and coated forms, Catalysts. 12 (2022) 1663.
[87] J. Fito, K.K. Kefeni, T.T.I. Nkambule, The potential of biochar-photocatalytic nanocomposites for removal of organic micropollutants from wastewater, Sci. Total. Environ. 829 (2022) 154648, https://doi.org/10.1016/J.SCITOTENV.2022.154648.
[88] A.S. Mestre, A.P. Carvalho, Photocatalytic degradation of pharmaceuticals carbamazepine, diclofenac, and sulfamethoxazole by semiconductor and carbon materials: a review, Molecules. 24 (2019) 3702.
[89] A. Kutuzova, T. Dontsova, W. Kwapinski, Application of TiO2-based photocatalysts to antibiotics degradation: cases of sulfamethoxazole, trimethoprim and ciprofloxacin, Catalysts. 11 (2021) 728.
[90] J.Y. Zhang, J. Ding, L.M. Liu, R. Wu, L. Ding, J.Q. Jiang, et al., Selective removal of sulfamethoxazole by a novel double Z-scheme photocatalyst: preferential recognition and degradation mechanism, Environ. Sci. Ecotechnol. 17 (2024) 100308.
[91] J. Khodayari, K. Zare, O. Moradi, M. Kalaee, N.M. Mahmoodi, A novel synthesis of a calix [4]arene, MIL-101 (Fe), and copper (II) oxide nanocomposite (Calix/MIL-101 (Fe)/CuO): synthesis, characterization, degradation, and pollutant removal ability, ChemistrySelect. 9 (2024) e202403168.
[92] Al-Nuaim MA, A.A. Alwasiti, Z.Y. Shnain, The photocatalytic process in the treatment of polluted water, Chem. Pap. 77 (2023) 677–701.
[93] M. Manasa, P.R. Chandewar, H. Mahalingam, Photocatalytic degradation of ciprofloxacin & norfloxacin and disinfection studies under solar light using boron & cerium doped TiO2 catalysts synthesized by green EDTA-citrate method, Catal. Today 375 (2021) 522–536, https://doi.org/10.1016/j.cattod.2020.03.018.
[94] G.K. Teye, J. Huang, Y. Li, K. Li, L. Chen, W.K. Darkwah, Photocatalytic degradation of sulfamethoxazole, nitenpyram and tetracycline by composites of core shell g-C3N4@ ZnO, and ZnO defects in aqueous phase, Nanomaterials 11 (2021) 2609.
[95] Z. Fang, Z.Z. Lin, P. Chen, M. Feng, H. Liu, Z. Xiao, et al., Enhanced photochemical degradation and transformation of ciprofloxacin in a UV/calcium peroxide system: pH effects, defluorination kinetics, and different components numerical analysis, J. Clean. Prod. 414 (2023).
[96] M.G. Alalm, D.C. Boffito, Mechanisms and pathways of PFAS degradation by advanced oxidation and reduction processes: a critical review, Chem. Eng. J. 450 (2022) 138352.
[97] J. Martini, J.O. Ighalo, E.C. Emenike, J. Georgin, E. Carissimi, Degradation of the Antibiotic Sulfamethoxazole by Ozonation: A Comprehensive Review (2024).
[98] J. Yao, Y. Xu, H. Yang, Z. Ren, L. Wu, Y. Tang, Identifying the metallic state of Rh catalyst on boron nitride during partial oxidation of methane by using the product molecule as the infrared probe, Catalysts. 12 (2022) 1146.
[99] M. Cao, Y. Shen, Z. Yan, Q. Wei, T. Jiao, Y. Shen, et al., Extraction-like removal of organic dyes from polluted water by the graphene oxide/PNIPAM composite system, Chem. Eng. J. 405 (2021) 126647.
[100] J. Li, S. Li, Z. Cao, Y. Zhao, Q. Wang, H. Cheng, Heterostructure CoFe2O4/kaolinite composite for efficient degradation of tetracycline hydrochloride through synergetic photo-Fenton reaction, Appl. Clay. Sci. 244 (2023) 107102.
[101] S. Sattar, M. Yahya, S. Aslam, R. Hussain, S.M.M. Shah, Z. Rauf, et al., Environmental occurrence, hazards, and remediation strategies for the removal of cadmium from the polluted environment, Results. Eng. 25 (2025) 104322.
[102] L. Ding, R. Mao, S. Ma, X. Guo, L. Zhu, High temperature depended on the ageing mechanism of microplastics under different environmental conditions and its effect on the distribution of organic pollutants, Water. Res. 174 (2020) 115634.
[103] H. Ghazal, E. Koumaki, J. Hoslett, S. Malamis, E. Katsou, D. Barcelo, et al., Insights into current physical, chemical and hybrid technologies used for the treatment of wastewater contaminated with pharmaceuticals, J. Clean. Prod. 361 (2022) 132079.
[104] M. Mittal, S. Tripathi, D.K. Shin, Biopolymeric nanocomposites for wastewater remediation: an overview on recent progress and challenges, Polymers. (Basel) 16 (2024) 294.
[105] M. Osman, I. Qureshi, Review of photovoltaic and concentrated solar technologies including their performance, reliability, efficiency and storage, Results. Eng. (2025) 104424.
[106] H. Khan, M.U.H. Shah, Modification strategies of TiO2 based photocatalysts for enhanced visible light activity and energy storage ability: a review, J. Environ. Chem. Eng. (2023) 111532.
[107] A.B. Ponnusami, S. Sinha, H. Ashokan, M.V. Paul, S.P. Hariharan, J. Arun, et al., Advanced oxidation process (AOP) combined biological process for wastewater treatment: a review on advancements, feasibility and practicability of combined techniques, Environ. Res. 237 (2023) 116944.
[108] P.K. Pandis, C. Kalogirou, E. Kanellou, C. Vaitsis, M.G. Savvidou, G. Sourkouni, et al., Key points of advanced oxidation processes (AOPs) for wastewater, organic pollutants and pharmaceutical waste treatment: a mini review, ChemEngineering 6 (2022) 8.
[109] P. Mahbub, M. Duke, Scalability of advanced oxidation processes (AOPs) in industrial applications: a review, J. Environ. Manage 345 (2023) 118861.